JOURNAL OF SPACECRAFT AND ROCKETS
Vol. 47, No. 3, May–June 2010

Electrodynamic Tether Applications and Constraints

Juan R. Sanmartin*
Universidad Politécnica de Madrid, 28040 Madrid, Spain
Enrico C. Lorenzini†
University of Padova, 35131 Padova, Italy
and
Manuel Martinez-Sanchez‡
Massachusetts Institute of Technology, Cambridge, Massachusetts 02139

DOI: 10.2514/1.45352

Propulsion and power generation by bare electrodynamic tethers are revisited in a unified way and issues and constraints are addressed. In comparing electrodynamic tethers, which do not use propellant, with other propellant-consuming systems, mission duration is a discriminator that defines crossover points for systems with equal initial masses. Bare tethers operating in low Earth orbit can be more competitive than optimum ion thrusters in missions exceeding two–three days for orbital deboost and three weeks for boosting operations. If the tether produces useful onboard power during deboost, the crossover point reaches to about 10 days. Power generation by means of a bare electrodynamic tether in combination with chemical propulsion to maintain orbital altitude of the system is more efficient than use of the same chemicals (liquid hydrogen and liquid oxygen) in a fuel cell to produce power for missions longer than one week. Issues associated with tether temperature, bowing, deployment, and arcing are also discussed. Heating/cooling rates reach about 4 K/s for a 0.05-mm-thick tape and a fraction of Kelvin/second for the ProSEDS (0.6-mm-radius) wire; under dominant ohmic effects, temperatures are over 200 K (night) and 380 K (day) for the tape and 320 and 415 K for that wire. Tether applications other than propulsion and power are briefly discussed.

Nomenclature

A_t	=	tether cross-sectional area, m^2
B_0	=	ambient magnetic field, T
c_{ch}	=	exhaust velocity of chemical rocket, m/s
E_m	=	motional electric field, V/m
$\tilde{E}_m$	=	normalized motional field defined in Eq. (19), V/m
F_M	=	magnetic force on tether, N
h	=	tape thickness, m
I	=	tether current, A
I_{OML}	=	orbital-motion-limited current, A
I_{av}	=	length-averaged bare tether current, A
i	=	current normalized with short-circuit current
L	=	tether length, m
L_B	=	length of anodic segment, m
L_{ins}	=	length of tether segment insulated for thrusting, m
L^*	=	length characterizing ohmic effects, m
M_D	=	mass of drag subsystem, kg
M_{Th}	=	mass of thrust subsystem, kg
m_t	=	tether mass, kg
N_0	=	ambient electron density, m^{-3}
p	=	tether cross-sectional perimeter, m
R (R_{max})	=	wire radius (maximum radius for orbital-motion-limited regime), m
R_{eq}	=	equivalent radius of noncircular cross section, m
r_{sh}	=	radius of Debye sheath, m
s	=	distance along tether from its anodic end, m
$T(s)$	=	tether temperature, K
v_{orb}	=	orbital velocity, m/s
$\dot{W}_M$	=	magnetic force power, W
$\dot{W}_e$	=	supply power, W
w	=	tape width, m
y	=	lateral tether deflection, m
Z_{load}	=	load impedance, Ω
Z_t	=	tether resistance, Ω
α	=	inverse specific power of power source, kg/W
α_t	=	full tether-hardware/tether-mass ratio
ΔV	=	tether bias, V
$\delta\dot{W}_{th}$	=	power heating a tether length element δs, W
η_{el}	=	electric thrust efficiency
η_g	=	tether efficiency for power generation
λ_{De}	=	Debye length of ambient plasma, m
ρ	=	tether density, kg/m^3
σ_B	=	Stefan–Boltzmann constant (5.6704×10^{-8} W/m^2 K^4)
σ_c	=	tether conductivity $1/\Omega m$
τ_b	=	propellant burn time, s
Φ_P	=	cylindrical probe bias, V

Subscripts

A, B, C	=	anodic-end, zero-bias, and cathodic-end points

Received 8 May 2009; revision received 8 January 2010; accepted for publication 24 January 2010.

*Professor, Department of Applied Physics, Plaza Cardenal, Cisneros 3. Senior Member AIAA.
†Professor, Department of Mechanical Engineering, Via Venezia 1. Senior Member AIAA.
‡Professor, Department of Aeronautics and Astronautics, 77 Massachusetts Avenue. Senior Member AIAA.

I. Introduction

THE development of tether technology for space has already experienced 18 suborbital and orbital flights, beginning with the Gemini–Agena tether experiments in 1967. Eight of those flights used electrodynamic tethers, starting from suborbital flights in 1980, as shown in Table 1 with relevant flight data [1,2]. One additional electrodynamic tether system, ProSEDS, was developed and built by NASA but was not launched into space in 2003 because of unfortunate circumstances.

Electrodynamic tether (ED—tether) systems have evolved over the last three decades through the development of different technologies for the main components. Current exchange with the ambient rarefied plasma was soon identified as a technological bottleneck. The TSS1 and TSS1R tether missions used a big

Table 1 Tethered satellite missions flown to date

Name	Date	Orbit	Length	Agency	Comments
Gemini 11	1967	LEO	30 m	NASA	Spin stable 0.15 rpm
Gemini 12	1967	LEO	30 m	NASA	Local vertical, stable swing
H-9M-69[a]	1980	Suborbital	500 m	NASA	Partial deployment
S-520-2[a]	1981	Suborbital	500 m	NASA/ISAS	Partial deployment
Charge-1[a]	1983	Suborbital	500 m	NASA/ISAS	Full deployment
Charge-2[a]	1984	Suborbital	500 m	NASA/ISAS	Full deployment
Oedipus-A	1989	Suborbital	958 m	Canadian NRC/NASA	Spin stable 0.7 rpm, magnetic field aligned
Charge-2B[a]	1992	Suborbital	500 m	NASA	Full deployment
TSS-1[a]	1992	LEO	260 m	NASA/Italian Space Agency	Partial deployment, retrieved
SEDS-1	1993	LEO	20 km	NASA	Downward full deployment, swing, and cut
PMG[a]	1993	LEO	500 m	NASA	Upward deployed
SEDS-2	1994	LEO	20 km	NASA	Full deployment, local vertical stable
Oedipus-C	1995	Suborbital	1 km	Canadian NRC/NASA	Spin stable 0.7 rpm, magnetic field aligned
TSS-1R[a]	1996	LEO	19.6 km	NASA/Italian Space Agency	Close to full deployment, severed by arcing
TiPS	1996	LEO	4 km	NRO/NRL	Long-life tether on-orbit (survived 12 years)
ATEx	1999	LEO	6 km	NRL	Partial deployment
ProSEDS[a]	2003	LEO	15 km	NASA	Hardware built but not flown
MAST	2007	LEO	1 km	NASA	Did not deploy
YES2	2007	LEO	30 + km	ESA	Full deployment

[a]Electrodynamic tether mission.
[b]ISAS is the Institute of Space and Astronautical Science, NRC is the National Research Council, NRO is the National Reconnaissance Office, and NRL is the Naval Research Laboratory.

conductive sphere at the end of the tether as the anode where electrons are collected from the ionosphere and used an electron gun as the cathode to eject those electrons into space at the other tether end [3–5]. A second option, adopted in one of the tether flights [the plasma motor generator (PMG)], consisted of using plasma contactors (hollow cathodes) at both tether ends for either electron collection or ejection [6].

In the early 1990s, the bare-tether concept was proposed as providing an electron-collecting anode limited by neither space charge nor magnetic guiding effects and thus being more efficient than a big conductive sphere [7,8]. The ProSEDS mission was indeed designed and built by NASA and its contractors to test the bare-tether concept in space. The goal of that system was to demonstrate the collection of a high electron current and, consequently, the generation of a significant Lorentz force to rapidly drag down the mother platform, a Delta second stage to which the tether was attached [9].

Although bare electrodynamic tethers may be used in a variety of applications with unique benefits, as in operations of radiation belt remediation (RBR), generation of electron beams to produce artificial auroras, excitation of fronts of Alfven waves or solar sailing, the fundamental area of application is propellantless transportation [10]. This can be synthesized conceptually as exchanging momentum (and energy) between a planetary magnetosphere and the tether system, thereby decreasing or increasing the momentum of the tether system. The present paper discusses the basic applications in the area of propellantless propulsion related to reboosting space platforms, deorbiting dead satellites and spent stages, and generating electrical power in space [11].

The basic concepts in conductive space tethers and results from theory, numerical simulations, and laboratory tests on bare-tether current collection are reviewed in the following two sections. Design parameters characterizing tether performance are presented next. We then review drag, thrust, and power generation modes of operation, as well as RBR and e-beam generation applications. Basic constraints on tether performance arising from heating, bowing, and environment interactions; tether deployment; and issues for future development are discussed in dedicated sections. Conclusions are summarized in a final section.

II. Electrodynamic Tether Basics

A nonrelativistic transformation relates throughout the electric fields in frames moving with spacecraft (SC) and local ambient plasma:

$$\bar{E}\ (\text{tether frame}) - \bar{E}\ (\text{plasma frame}) \equiv \bar{E}_m = (\bar{v}_{\text{orb}} - \bar{v}_{\text{pl}}) \times \bar{B}_0 \tag{1}$$

where the planetary magnetic field $\bar{B}_0$ is common to both frames, and where $\bar{v}_{\text{orb}}$ and $\bar{v}_{\text{pl}}$ are the velocities of SC (and tether) and plasma, assumed to be corotating in the following. For no significant currents in the highly conductive ambient plasma, the electric field outside the tether will vanish in the corotating frame; in the tether frame, there is then an outside field $\bar{E}_m$ that will drive a current $\bar{I}$ inside the tether with $\bar{I} \cdot \bar{E}_m > 0$ in the case of a passive tether system. [The field inside the tether, in its own frame, relates directly to current through Ohm's law; Eq. (1) then yields the irrelevant inside field in the plasma frame.]

The Lorentz force on an insulated tether of length L carrying a uniform current reads $L\bar{I} \times \bar{B}_0$. With Newton's third law valid for magnetic forces between steady-current systems, a net power loss is seen to occur in the tether–plasma interaction:

$$L\bar{I} \times \bar{B}_0 \cdot \bar{v}_{\text{orb}} + (-L\bar{I} \times \bar{B}_0) \cdot \bar{v}_{\text{pl}} \equiv -\bar{I} \cdot \bar{E}_m L < 0 \tag{2}$$

which is (Lorentz) power naturally feeding the tether electric circuit [12]. The Lorentz force would be a drag for $\bar{v}_{\text{orb}}$ in the direction of the SC velocity relative to the plasma, $\bar{v}_{\text{orb}} - \bar{v}_{\text{pl}}$, which is the case for circular equatorial orbits, either retrograde or prograde at radius $a < a_s$, where a_s is the stationary-orbit radius for the planet considered; Fig. 1 shows the directions of relative velocity and Lorentz force in the general prograde case. For a vertical tether in low Earth orbit (LEO) and a nontilted centered magnetic dipole model (B_0 northward, E_m upward), a typical motional field is

$$E_m = v_{\text{orb}} B_0 \sim 7.5\ \text{km/s} \times 0.2\ \text{G} = 150\ \text{V/km}$$

with drag and power reading as follows.

Westward Lorentz drag:

$$F_M = LIB_0$$

Drag power:

$$\dot{W}_M = F_M v_{\text{orb}} = IE_m L$$

Because of both a rapid spin Ω_J (about a 10 h period) and low mean density ρ_J (1.33 g/cm^3), the stationary orbit in Jupiter is one-third the relative distance for Earth

$$a_s = R_J (4\pi G \rho_J / 3\Omega_J^2)^{1/3}$$

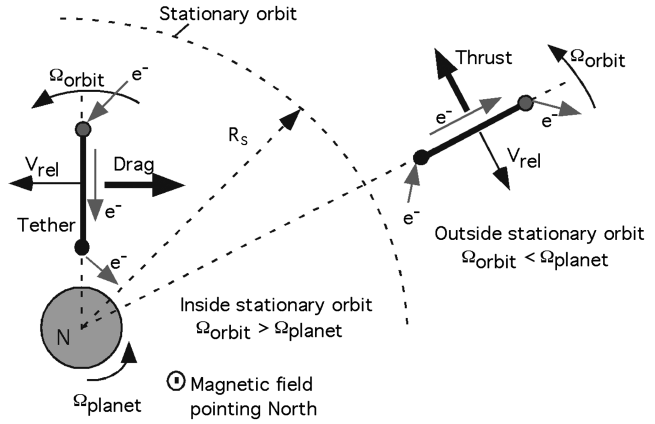

Fig. 1 Drag or thrust for electrodynamic tether subjected to motional emf. Corotation reaches beyond the stationary orbit in Jupiter's magnetosphere.

or $a_s = 2.24$ times the Jovian radius R_J. In turn, the magnetic field at its surface is greater than at Earth's by one order of magnitude. As a result, there is magnetospheric plasma corotating beyond a_s. The Lorentz force on a tether in prograde Jovian orbit beyond a_s would be a thrust [13].

In the case of a polar orbit with a nontilted magnetic dipole model, which is actually a model fitting Saturn, both SC velocity and magnetic field lie in the orbital plane. If the tether is kept lying or rotating in that same plane, the Lorentz force, though tending to reduce the orbit inclination, will exert no mechanical power; electrical power, however, is extracted from the corotating plasma through the second term on the left-hand side of Eq. (2) [14]. On the other hand, for a tether kept perpendicular to the orbital plane, the gravity gradient is compressive, making the use of rigid short booms necessary [15].

In general (for nonzero orbital inclination or a realistic magnetic model), $\bar{B}_0$ has components in the orbital plane in addition to a perpendicular component $B_{0\perp}$. The relations for current driven by the motional field and drag power remain valid in terms of $B_{0\perp}$, and the motional field component perpendicular to the orbit just produces a negligible potential difference across the thin tether. The perpendicular Lorentz force, however, pushes the tether off the orbital plane and may lead to a coupled in-plane/off-plane unstable periodic motion, with the period of the orbit, with the growth rate depending sharply on the ratio of masses at the tether ends [16].

III. Bare Electrodynamic Tethers

ED-tether operation requires effective electrical contact with the ambient plasma. State-of-the-art hollow cathodes are indeed effective in establishing cathodic contact: they expel little xenon along with the electrons and require bias of tens of volts only, thus resulting in negligible contact impedance [17–19]; alternative cathodes are actively pursued nonetheless [20,21]. In turn, the problem of anodic contact with the highly rarefied ionospheric plasma (density being about $10^{12}/\mathrm{m}^3$ at most), which was previously considered to be a bottleneck, was solved in 1991 when it was proposed that, instead of using a large end collector, the tether be left bare of insulation to allow it to collect electrons over the resulting positively polarized segment, as shown in Fig. 2, as a giant cylindrical Langmuir probe in the so-called orbital-motion-limited (OML) regime [7,8]. Collection is efficient because the cross-sectional dimension is small, while the collecting area is large because the anodic segment may be tens of kilometers long.

The maximum current collected by a round cylindrical Langmuir probe in a quiescent unmagnetized plasma is the OML current, which for high positive bias $e\Phi_p \gg kT_e$ reads

$$I_{\mathrm{OML}} \approx I_{\mathrm{th}} \sqrt{\frac{4e\Phi_p}{\pi kT_e}} = eN_0 \frac{Lp}{\pi} \sqrt{\frac{2e\Phi_p}{m_e}} \propto p, \qquad p = 2\pi R \tag{3}$$

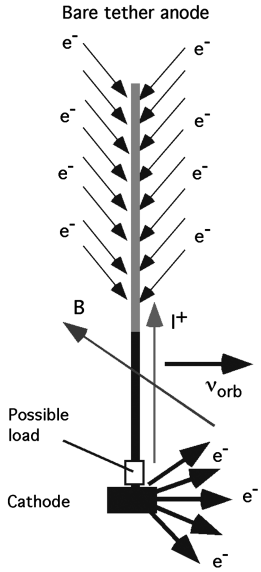

Fig. 2 Sketch of bare-tether anode operating in the drag/power generation mode.

where $I_{\mathrm{th}} = 2\pi RLeN_0\sqrt{kT_e/2\pi m_e}$ is the random current in the ambient plasma. The high-bias OML law, when valid, is robust, the ratio $I_{\mathrm{OML}}/I_{\mathrm{th}}$ being independent of both Debye and temperature ratios, R/λ_{De} and T_i/T_e; of the ambient ion distribution function; and of the ambient electron distribution if isotropic. Its domain of validity is given by a single condition:

$$R \le R_{\max} \equiv \lambda_{\mathrm{De}} \tilde{R}_{\max}(e\Phi_p/kT_e, T_i/T_e) \tag{4}$$

As shown in Fig. 3 (from [22]), at the high values of the bias ratio $e\Phi_p/kT_e$ of interest for tethers, $R_{\max}$ is close to the Debye length λ_{De} for a typical ionospheric T_i/T_e ratio about unity and is about $0.3\lambda_{\mathrm{De}}$, however, for $T_i = 0.3T_e$. For $R \ge R_{\max}$, the current reads [23]

$$\frac{I}{I_{\mathrm{OML}}(p)} = G\left(\frac{R}{\lambda_{\mathrm{De}}}, \frac{e\Phi_p}{kT_e}, \frac{T_i}{T_e}\right) < 1 \tag{5}$$

with the function G weakly dependent on bias and roughly dependent on a single variable, $(R/\lambda_{\mathrm{De}}) - \tilde{R}_{\max}(T_i/T_e)$. As shown in Fig. 4

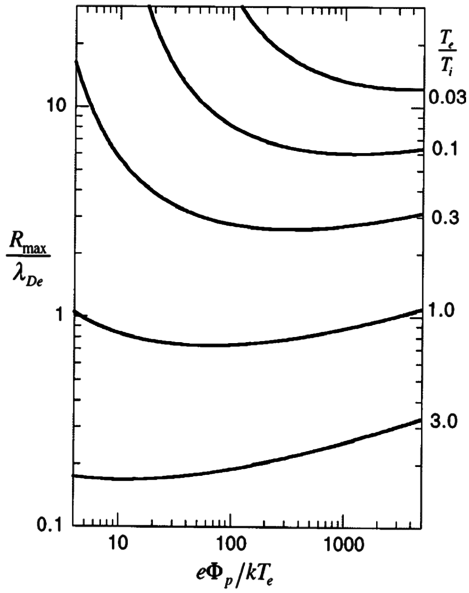

Fig. 3 Normalized maximum radius for OML validity versus bias and temperature ratios. Reprinted with permission from [22]; copyright 1999, American Institute of Physics.

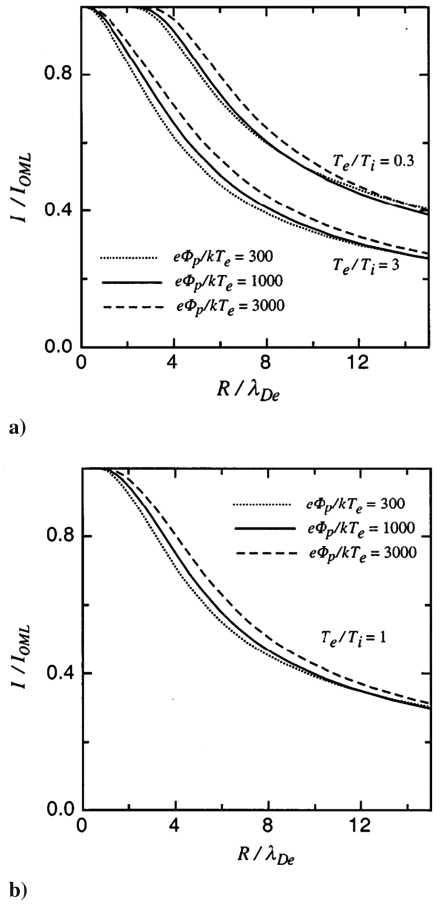

Fig. 4 Normalized current for $R > R_{max}$ for several values of bias and temperature ratios. Reprinted with permission from [23]; copyright 2000, American Institute of Physics.

(from [23]), G in Eq. (5) drops to a value of 0.9 at $R \approx 3R_{max}$ for $T_i = T_e$; the lower T_i is, the faster G drops with increasing R/R_{max}.

For $T_i = T_e$ excellent detailed agreement has been found [24] between the (asymptotic) analytical results in [22,23] and numerical results from both steady-state Vlasov calculations [25] and particle-in-cell simulations [26]. The potential $\Phi(r)$ behaves as $\Phi \sim \ell_n\, r$ in a large probe neighborhood free of space-charge effects because of the high bias, and as $\Phi \sim 1/r$ at large enough distance r, and in between, $r^2\Phi$ presents a minimum at a point outside the sheath and a maximum at a point well inside. The density itself shows a minimum at this point and a maximum closer to the probe. Agreement is found for R close to, but below, R_{max} on values and positions of density minimum and maximum; on the Debye sheath radius r_{sh}; and on the $\Phi/\ell_n\, r$ ratio in a neighborhood of the probe. There is also agreement on broad parametric laws for density minimum, current beyond the OML regime as given by Eq. (5), and sheath radius for $R \ll \lambda_{De}$ [24]:

$$1.53\left[1 - 2.56\left(\frac{\lambda_{De}}{r_{sh}}\right)^{4/5}\right]\left(\frac{r_{sh}}{\lambda_{De}}\right)^{4/3} \ell_n\left(\frac{r_{sh}}{R}\right) \approx \frac{e\Phi_p}{kT_e} \qquad (6a)$$

For $R = R_{max} \approx \lambda_{De}$ and $T_i \approx T_e$, the sheath law is [22,21]

$$r_{sh}/R_{max} \approx r_{sh}/\lambda_{De} \approx 2\sqrt{e\Phi_p/kT_e} \qquad (6b)$$

The OML-current law (3) is also valid for any convex cross-sectional shape, where p is its actual perimeter [27]. Laws (4) and (5) are valid too, except that certain *equivalent radius* $R_{eq} \neq p/2\pi$ must be calculated and used to replace R. Because of the high bias, determining R_{eq} for each convex cross section just requires solving the Laplace equation between an arbitrarily large circle and the cross section, at relative bias Φ_p, at its center, which is a classical calculation for the capacity per unit length of a coaxial line [28]. For the case of a thin tape of width w, one finds $R_{eq} = w/4 \approx p/8$. Note that a tape that collects the same OML current as a round wire of equal cross-sectional perimeter will be much lighter, with the optimal tether thus presenting three disparate dimensions: $L \gg w \gg h$ (*tape thickness*).

Further, the law (3) would still hold to great accuracy for concave shapes [for which we would have $I < I_{OML}(p)$, irrespective of cross-sectional size] if the actual perimeter is replaced by the perimeter p_{eq} of the minimum-perimeter cross-sectional envelope [28]. Multiple numerical calculations and laboratory tests have been carried out in trying to determine whether all above results would hold in a flowing magnetized plasma at the mesothermal speed of a LEO orbit, which barely breaks the ambient electron-distribution isotropy, and for ambient electron gyroradius l_e well above both R_{eq} and λ_{De} [29–33]. Results need verification in space because conclusive laboratory tests would need to reproduce LEO values for all relevant ratios (T_i/T_e, $m_i v_{orb}^2/kT_e$, and l_e/λ_{De}) and to allow current collection under collisionless and two-dimensional (2-D) conditions for a range of bias and Debye ratios.

Actually, bare-tether current collection by the 400-m-long lattice of tensioning rods for each (40-m-long) mast in the International Space Station solar array was used to explain current balance in the station when repeatedly passing south of Australia in early 2001 [34]. Bare-tether collection will also be tested in the summer of 2010 by a dedicated sounding-rocket mission (S-520-25) of the Japanese Aerospace Exploration Agency (JAXA), according to a double-probe scheme designed by one author of the present paper [35]. A tape tether (hollow cathode) will first be connected to the positive (negative) terminal of a battery supply at different settings, used for bias, because a suborbital rocket allows too small a motional-field emf $E_m L$; electrons collected by the tape will cross the supply and escape at the hollow cathode. Then the tape (a short boom) will be connected to the negative (positive) supply terminal; electrons collected by the boom will cross the supply and leak out from the tape at the rate of ion impact. Figure 5 (from [35]) shows the connection arrangements. Bare-tether collection will thus be tested for both electrons and ions over a range of probe bias for different cross-sectional shapes and for sizes within and beyond the OML regime.

At the high-bias conditions of interest for bare tethers, the sheath radius is much larger than R (or R_{eq}) in both Eqs. (6a) and (6b). Testing OML collection by cylinders then requires not just a length $L \gg 2R$, but the much stricter condition $L \gg 2r_{sh}$. A recent proposal for testing OML in a CubeSat experiment [36] would use tapes so short, however, that collection would not occur under cylindrical 2-D geometry, but rather under 3-D conditions.

Note that a tether is a singular Langmuir probe because bias and current will vary along its length, but the extremely large length-to-radius ratio allows using uniform-bias results at each local tether section. Both F_M and $\dot{W}_M$ now involve the current I_{av} averaged over the tether length. In the absence of ohmic effects to be discussed in

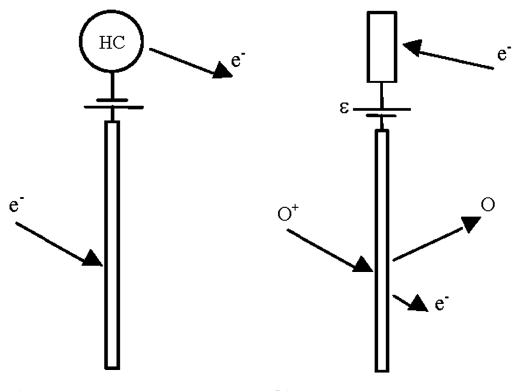

Fig. 5 Sketch of electric connections for OML-current testing in the JAXA S-520-25 rocket mission. Hollow-cathode (HC), tape, and battery supply for voltage ε, are involved in a first stage (a); tape, battery supply, and short boom, in a second stage (b); from [35].

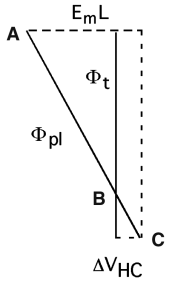

Fig. 6 Diagram of tether (Φ_t) and plasma (Φ_{pl}) potential lines, both in the tether frame, with $\Delta V = \Phi_t - \Phi_{pl}$ for drag mode and negligible ohmic effects; bias at the cathodic end C is the hollow-cathode bias ΔV_{HC}.

the next section, and as shown in Fig. 6, the tether is equipotential in its own frame, whereas the potential outside varies linearly at the E_m rate. The local bias $\Phi_p \equiv \Delta V$ then decreases linearly with distance from the anodic end, from a maximum $E_m L$ there to a near-zero negative value ΔV_C at the hollow cathode at end C. Current increases from zero at the anodic end A to a maximum at zero bias (point B), with ion collection over the cathodic segment BC being negligible. If collection is OML everywhere, one finds

$$I_{\rm av}^{\rm OML} = \frac{2}{5} \times eN_0 \frac{Lp}{\pi} \sqrt{\frac{2eE_m L}{m_e}}$$

with the maximum current $I_C \approx I_B = 5I_{\rm av}/3$.

A simple figure of merit for the Lorentz drag $I_{\rm av}^{\rm OML} L B_0$ on a tether would be its ratio to the drag by hypothetical neutrals with the mass and density of ions on a body of equal front-area $2RL$, as given by a standard aerodynamics law. That ratio reads

$$\frac{I_{\rm av}^{\rm OML} L B_0}{2RLc_D m_i N_0 v_{\rm orb}^2/2} \equiv \frac{4\sqrt{2}}{5c_D} \sqrt{\frac{m_i}{m_e}} \left(\frac{\Omega_i L}{v_{\rm orb}}\right)^{3/2}$$

where the drag coefficient c_D is typically about 2. The ratio above is usually an extremely large number. For oxygen, the square root of the ion-to-electron mass ratio $\sqrt{m_i/m_e}$ is about 171; for typical LEO values (ion gyrofrequency $\Omega_i \sim 200$/s and $v_{\rm orb} \sim 7.5$ km/s), a length $L \sim 10$ km yields a ratio of order of 10^6. This means that Lorentz drag from weakly ionized plasma can be effective where the neutrals' drag is negligible.

IV. Tether-Circuit Design Parameters

In addition to the basic ratios for the local collection law ($R_{\rm eq}/R_{\rm max}$ and $p/R_{\rm eq}$), there is a number of dimensionless design parameters in the overall electric tether circuit affecting performance, a fundamental one concerning the extent of ohmic effects. In the absence of an active power system, the current is limited by its short-circuit value $\sigma_c E_m A_t$, where A_t is the cross-sectional area arising from the tether resistance $Z_t \equiv L/\sigma_c A_t$. A characteristic length L^* gauges ohmic effects for bare tethers [7,8]:

$$\frac{4}{3} eN_0 \frac{L^* p}{\pi} \sqrt{\frac{2eE_m L^*}{m_e}} \equiv \sigma_c E_m A_t = \frac{E_m L}{Z_t} \tag{7}$$

$$L^* \propto E_m^{1/3} \left(\frac{\sigma_c A_t}{N_0 p}\right)^{2/3} \tag{8}$$

The average current can be written as $I_{\rm av} \equiv i_{\rm av} \sigma_c E_m A_t$, where, for drag operation, $i_{\rm av}$ is a function of just L/L^*,

$$\frac{I_{\rm av}\,({\rm drag})}{\sigma_c E_m A_t} = i_{\rm av}\left(\frac{L}{L^*}\right) \tag{9}$$

with the current $i_{\rm av}$ approaching 1 at large L/L^* and approaching

$$i_{\rm av} = I_{\rm av}^{\rm OML}/(\sigma_c E_m A_t) \equiv 3(L/L^*)^{3/2}/10 \tag{10}$$

at small L/L^*. Collection performance per unit tether mass would be optimum for $L \gg L^*$, when current attains its maximum value. Since length L^* varies as $R^{2/3}$ for a round-wire tether of radius R, and as $h^{2/3}$ for a thin tape of area $A_t = wh$, as seen in Eq. (8), moving from round wires to tapes improves performance, as pointed out in the previous section. Note that a large ratio L/L^* is equivalent to negligible contact impedance for bare-tether collection.

Consider an increasing ratio L/L^* for given tether and motional field E_m, with L^* decreasing as plasma density increases and with the tether potential line being straight, as shown in Fig. 6 in the small L/L^* limit (no ohmic-effects limit). As L^* decreases all the way to a value of $\frac{1}{4}L$, the anodic bias ΔV_A reaches down to a value $E_m L^*$, and the normalized current i_B ($\approx i_C$) reaches unity, with the vanishing bias point B lying near the bottom throughout. These values hold as L^* decreases beyond $\frac{1}{4}L$, whereas point B rises above the bottom, nonetheless keeping current $i_C \approx i_B = 1$, because collection of the slow-moving ions over the cathodic segment BC at the small hollow-cathode bias is negligible [37]. These changes are described by equations

$$\left(1 - \frac{L_B}{L}\right)(1 - i_B) = \frac{\Delta V_C}{E_m L} \approx 0 \tag{11a}$$

$$L_B/L^* = \xi_B(i_B) \tag{11b}$$

where L_B is the length of segment AB, and the function ξ_B equals $(2i_B)^{2/3}$ for small i_B and reaches 4 at $i_B = 1$; Eqs. (11a) and (11b) yield i_B and L_B/L as just functions of L/L^*.

For power generation, the tether circuit involves both the ratio L/L^* and a second ratio, $Z_{\rm load}/Z_t$, where $Z_{\rm load}$ is the impedance characterizing a power load located at the cathodic end between tether and hollow cathode (Fig. 2). The normalized current would, in principle, read

$$\frac{I_{\rm av}({\rm power})}{\sigma_c E_m A_t} = i_{\rm av}\left(\frac{L}{L^*}, \frac{Z_{\rm load}}{Z_t}\right) \tag{9$\prime$}$$

Generated power would be maximum at some efficiency:

$$Z_{\rm load} I_C^2/(I_{\rm av} E_m L) \equiv \eta_g(L/L^*, Z_{\rm load}/Z_t)$$

To invert both anodic- and cathodic-end locations, and thus current direction so as to produce thrust, both a power source and the hollow cathode must lie at the top, with electrons flowing upward (for eastward orbits in LEO); this arrangement is shown in Fig. 7. The normalized current would now read

$$\frac{I_{\rm av}({\rm thrust})}{\sigma_c E_m A_t} = i_{\rm av}\left(\frac{L}{L^*}, \frac{L_{\rm ins}}{L^*}, \frac{\dot{W}_e}{\sigma_c E_m^2 A_t L}\right) \tag{9$\prime\prime$}$$

where $\dot{W}_e$ is the electrical supply power, and $L_{\rm ins}$ is the length of a tether segment next to the top that must be insulated, because a fully bare tether would have low propulsive efficiency; the many electrons collected near the top (where bias would be largest) would do little push work and yet would consume energy from the power source.

As seen in the next section, comparing system-mass budgets brings in an ambient dimensionless ratio $\tilde{E}_m$ [see Eq. (19)] involving an inverse specific power parameter characterizing tethers,

$$\frac{\rho}{\sigma_c E_m^2} \approx 3.44 \left(\frac{150\ {\rm V/km}}{E_m}\right)^2 \frac{\rm kg}{\rm kW} \tag{12}$$

where we used values for aluminum and the inverse specific power α (in kilograms/kilowatt) of some required power source: solar array, fuel cell, or radioisotope thermal generator.

The magnetic field due to the tether current introduces an additional parameter characterizing reduced current collection by tethers. Strong reduction would roughly occur at tether points at which some average radius r^* of a magnetic separatrix modifying

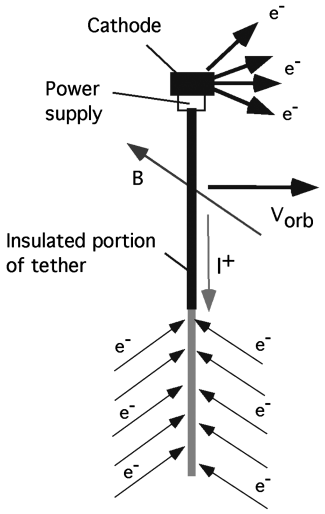

Fig. 7 Sketch of bare-tether anode operating in the thrust mode.

field topology in the cross-sectional plane exceeds the sheath radius r_{sh} [38,39]:

$$r_{sh} < r^* \equiv I/(2\pi\varepsilon_0 c^2 B_0) \tag{13}$$

Actually, in the case of thin tapes, ohmic effects severely limit current and separatrix radius and make self-field effects typically negligible [40]. For an equivalent radius $R_{eq} = w/4 \sim R_{max}$, we use Eq. (6b) and write $I \equiv i\sigma_c E_m A_t$; condition (13) then reads

$$\sqrt{\frac{e\Delta V}{kT_e}} < \frac{\sigma_c v_{orb}}{4\pi\varepsilon_0 c^2}\frac{A_t}{R_{eq}} i \tag{14}$$

For an aluminum tape in LEO ($v_{orb} \approx 7.5$ km/s and $kT_e = 0.1$–0.15 eV), with thickness $h = 0.05$ μm as with the tape for the 2010 JAXA mission and maximum $i \approx 1$, Eq. (14) shows collection reduced when bias is less than about $3V$, i.e., over a tether segment both short and weakly biased, which would thus collect very little current anyway.

A round wire of radius $R < 0.5$ mm in LEO i.e., R much less than λ_{De} at both night ($\sim$9 mm) and day ($\sim$3 mm), with $\sqrt{kT_e/e\Delta V} \times r_{sh}/\lambda_{De} \sim 1$–$2$ typically in Eq. (6b), would also present negligible self-field reduction at either condition. For $R \sim 1$ mm, sensible reduction might occur in daytime (but not at night). A wire of radius $R > 3$ mm would present current reduction during the day; with tether mass $m_t \propto LR^2$, however, use of Eq. (8) shows that such a wire at night would be either over 1 t heavy or quite inefficient ($i_{av} \ll 1$), even though not exhibiting self-field effects. Self-field effects for round tethers would be particularly negligible in Jupiter, outer radiation belt (as for RBR), or interplanetary space (as for electric sails later considered), where the very low plasma density implies that R is much less than λ_{De}, and both L/L^* and i_{av} are small for any reasonably sized tether.

V. Drag/Deorbiting Operation Mode

The most obvious application of an electrodynamic tether is as an end-of-life system to deorbit dead satellites and spent rocket stages, which are increasingly crowding the LEO region. The alternative device would be a solar-powered electric thruster [41]. A figure of merit for comparing these alternatives, in order to identify regions in the system-parameter domain in which an electrodynamic tether may be more desirable, would be the inverse specific mission impulse, i.e., the ratio between required drag-system mass M_D and deorbiting impulse $F\tau_b$ that either system must provide within some allotted burn time τ_b.

For an ion thruster as representative of electric propulsion, with M_D basically made of propellant consumed and power plant, that ratio reads

$$\frac{M_{elD}}{F_{el}\tau_b} \approx \frac{\dot{m}_{el}\tau_b + \alpha\dot{m}_{el}c_{el}^2/2\eta_{el}}{\dot{m}_{el}c_{el}\tau_b} = \frac{1}{c_{el}} + \frac{\alpha c_{el}}{2\eta_{el}\tau_b} \tag{15}$$

where η_{el}, c_{el}, and $\dot{m}_{el}$ are overall conversion efficiency (typically about 0.65), exhaust jet velocity, and ion mass flow rate. We ignored feed and storage and assumed full ionization for simplicity. Values of the inverse specific power α of a solar-power plant may be as high as 25 kg/kW if a dedicated plant is required and as low as 5 kg/kW otherwise. We shall consider the optimal thruster, for which the jet velocity minimizes the ratio in Eq. (15) for given α and burn time τ_b,

$$\frac{M_{elD,min}}{F_{el}\tau_b} = \frac{2}{c_{opt}} \equiv \sqrt{\frac{2\alpha}{\eta_{el}\tau_b}} \tag{16}$$

where the optimal exhaust velocity c_{opt} is Stuhlinger's characteristic velocity $\sqrt{2\eta_{el}\tau_b/\alpha}$.

For a tether, M_D would just be α_t times tether mass m_t, with the factor $\alpha_t > 1$ accounting for both tether and basic tether-related hardware. Using F_M we would have

$$\frac{M_{tD}}{F_M\tau_b} = \frac{\alpha_t\rho A_t L}{LI_{av}B_{0\perp}\tau_b} = \frac{\alpha_t\rho}{\sigma_c E_m^2}\frac{v_{orb}}{i_{av}\tau_b} \tag{17}$$

From Eqs. (16) and (17) we find

$$\frac{M_{tD}}{M_{elD,min}} = \sqrt{\frac{\eta_{el}\alpha v_{orb}^2}{2i_{av}^2\tilde{E}_m^4\tau_b}} \tag{18}$$

where we introduced the dimensionless motional field mentioned with Eq. (12),

$$\tilde{E}_m \equiv \sqrt{\alpha\sigma_c E_m^2/\alpha_t\rho} \tag{19}$$

with values just above (below) unity for aluminum and $\alpha_t \sim 2$–2.5 at the high (low) ends of LEO motional field and α ranges. The ratio in Eq. (18) reaches its minimum at large enough L/L^* when i_{av} approaches unity. For values $v_{orb} = 7.5 \times$ km/s and midrange $\alpha = 10$ kg/kW, that ratio lies below unity, proving tethers more mass-efficient than optimum ion thrusters for burn times as low as 2.5 days.

Actually, electric propulsion, which is less mass-efficient than chemical propulsion for short burning, might be left with no useful τ_b range when just mass efficiency is considered, as long as ambient conditions allow high i_{av} values. Setting the rocket exhaust velocity $c_{ch} < c_{opt}/2$ in Eq. (16) and a ratio above unity in Eq. (18) would yield a burn-time range for useful electric propulsion:

$$\frac{2\alpha c_{ch}^2}{\eta_{el}} < \tau_b < \frac{\eta_{el}\alpha v_{orb}^2}{2\tilde{E}_m^4 i_{av}^2} \tag{20}$$

Such a range does exist, but only under condition

$$i_{av} < \eta_{el} v_{orb}/(2c_{ch}\tilde{E}_m^2)$$

which is independent of α and reads as $i_{av} < 0.6$, typically in LEO.

Tethers may be shown to adjust to plasma density drops [42]. The average current $i_{av}(L/L^*)$ in Eq. (9) reads

$$i_{av}(L/L^*) \equiv 1 - L^*/L$$

for $L/L^* > 4$. Actually, this relation is also very accurate in the range of $2 < L/L^* < 4$, and Eq. (10) reasonably applies for L/L^* of, say, less than 0.5. The ratio L/L^* could decrease by a $10^{2/3}$ factor as the tether moves from day to night, corresponding to a typical density drop by a factor of 10. Choosing, say, $L/L^* > 9$ during the day (with point B lying high above the bottom at $L_B < 4L/9$ and i_{av} about unity), one would still have $i_{av} > 0.5$ at night.

VI. Power Generation Mode

A. Orbital Deboost While Powering

During a deorbiting operation, power may be freely generated at a power load, with some reduction in current and drag. Equation (11a) must now be modified to read [7,8]

$$\left(1-\frac{L_B}{L}\right)(1-i_B)=\frac{Z_{\rm load}}{Z_t}\,i_B \tag{21}$$

yielding [together with Eq. (11b)] both i_B and L_B/L, as well as $i_{\rm av}$ in Eq. (9′), as functions of L/L^* and $Z_{\rm load}/Z_t$. At large L/L^* and $Z_{\rm load}/Z_t=\mathcal{O}(1)$, some tether segment at the bottom might need to be insulated to keep ion collection negligible. Efficiency η_g and normalized generated power

$$\dot{w}_g\equiv\frac{Z_{\rm load}I_c^2}{\sigma_c E_m^2 A_t L}=\eta_g i_{\rm av},\qquad I_C\approx I_B \tag{22}$$

are also functions of L/L^* and $Z_{\rm load}/Z_t$. For large L/L^* with ohmic effects dominant, one finds [7,8]

$$\dot{w}_g\approx i_B(1-i_B) \tag{23a}$$

$$\eta_g\approx 1-i_B \tag{23b}$$

with maximum power being attained for $Z_{\rm load}=Z_t$, and with

$$i_B=i_{\rm av}=\eta_g=0.5,\qquad \dot{w}_g=0.25,\qquad L_B\ll L$$

In turn, for small L/L^*, with i_B also small and ohmic effects negligible, one has [7,8]

$$\dot{w}_g\approx i_B\left(1-\frac{L_B}{L}\right) \tag{24a}$$

$$\eta_g\approx\frac{L-L_B}{L-2L_B/5} \tag{24b}$$

using $\xi_B\approx(2i_B)^{2/3}$, as noted with Eq. (11b), maximum power is found to occur at

$$L_B=3L/5,$$

$$i_B=25i_{\rm av}/19=5\dot{w}_g/2=2Z_t/5Z_{\rm load}=0.5(3L/5L^*)^{3/2}\ll 1,$$

$$\eta_g=10/19\approx 0.526$$

Efficiency for maximum power is actually close to 0.5, whatever the ratio L/L^*.

Note that a plugged-in load impedance does reduce the Lorentz drag along with the average current. As just shown, for large L/L^*, $i_{\rm av}$ is reduced from a value of about unity for no load to the value of 0.5 at maximum power; for small L/L^*, $i_{\rm av}$ is reduced from the value in Eq. (10) for no load to a value that is smaller by a factor $\sqrt{3/5}\times 19/25\approx 0.589$ at maximum power. Hence, when comparing deorbit system mass for ion thrusters and tethers generating maximum power, one can just roughly use Eq. (18) with $i_{\rm av}$ reduced by a factor of about 0.5. Tethers generating power while deorbiting are thus more efficient than ion thrusters for burn times greater than about $4\times 2.5=10$ days.

B. Rocket-Balanced Stationary Power

Tethers might also be used to generate power when staying in orbit in an emergency mode, whether due to array failure or downtime for maintenance. Altitude loss may limit severely such a mode, however. On the other hand, altitude can be preserved by a combination ED-tether/chemical rocket, with the tether providing electric power and the rocket providing thrust to compensate the magnetic drag on the tether, as sketched in Fig. 8. It turns out that this combination is more mass fuel-efficient than using the rocket fuel to directly generate power in a fuel cell [11].

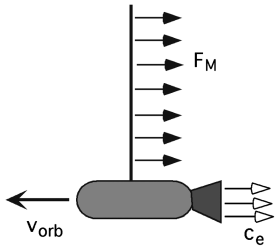

Fig. 8 Power generation by tether combined with rocket for Lorentz drag compensation.

Since rocket thrust must balance the Lorentz drag F_M to keep the SC velocity, the resulting Lorentz power

$$\dot{W}_M=F_M v_{\rm orb}=\dot{m}_{\rm ch}c_{\rm ch}v_{\rm orb} \tag{25}$$

is definitely greater than the rocket power output $\frac{1}{2}\dot{m}_{\rm ch}c_{\rm ch}^2$ by a factor $2v_{\rm orb}/c_{\rm ch}>3$ for $v_{\rm orb}\approx 7.5$ km/s and the greatest exhaust velocity $c_{\rm ch}\approx 4.5$ km/s for LOX–LH_2. It can be shown that the excess power in the combined tether/rocket system arises from the SC energy decrease at constant velocity, due to the rocket fuel-mass loss.

Fuel cells being lighter, however, the tether/rocket combination only saves mass for a long enough time τ_b,

$$\alpha_t\rho A_t L+\dot{m}_{\rm ch}\tau_b<\dot{m}_{\rm fc}\tau_b \tag{26}$$

with both systems being required to provide equal power:

$$\eta_{\rm fc}\dot{m}_{\rm fc}v_{\rm fc}^2/2=\eta_g\dot{m}_{\rm ch}c_{\rm ch}v_{\rm orb} \tag{27}$$

The fuel cell efficiency is about $\eta_{\rm fc}\sim 0.75$, and the energy per unit fuel mass liberated in a LOX–LH_2 cell is about 1.25×10^7 J/kg, which we write as $\frac{1}{2}v_{\rm fc}^2$ with $v_{\rm fc}\approx 5$ km/s. It follows from Eqs. (26) and (27) that the tether/rocket system is lighter for times satisfying

$$(\eta_g-b)i_{\rm av}\tau_b>\frac{\alpha_t\rho}{\sigma_c E_m^2}\frac{\eta_{\rm fc}v_{\rm fc}^2}{2}\left(b\equiv\frac{\eta_{\rm fc}v_{\rm fc}^2/2}{c_{\rm ch}v_{\rm orb}}\right) \tag{28}$$

Minimum mission time for the tether/rocket system to be lighter than a fuel cell system thus corresponds to maximum $(\eta_g-b)\,i_{\rm av}$. At large L/L^*, Eqs. (22), (23a), and (23b) yield $i_{\rm av}\approx 1-\eta_g$. With $b\approx 0.28$ typically in LEO, minimum time for Eq. (28) to hold then occurs at $\eta_g=0.64$ and $i_{\rm av}\approx 0.36$. Condition (28) now reads as $\tau_b>1$ week, typically [43]. Table 2 shows mission duration requiring equal masses for tether and standard-alternative systems, with the tether system being lighter for longer missions. Optimum-exhaust-speed ion thrusters at 10 kg/kW inverse specific power are compared to Al tethers in the ohmic-dominated regime and LEO conditions for deboost (with and without tether powering) and reboost [with tether-hardware mass at half of its power-subsystem mass (see Sec. VII)]. Powering by a LOX–LH2 fuel cell is compared to tether powering with its Lorentz drag balanced by LOX–LH2 rocket.

VII. Thrust Mode

In the thrust mode, with tethers as well as ion thrusters powered, a power-subsystem mass $\alpha\dot{W}_e$ must be added to M_{tD}. We then have

Table 2 Crossover durations for deboost reboost, and power generation

Mission	Mission duration times
Orbital deboost	2–3 days
Deboost at maximum tether powering	10 days
Reboost with optimum tether system	3 weeks
Rocket-balanced stationary power	1 week

$$\frac{M_{f\mathrm{Th}}}{F_M\tau_b} = \left(1 + \frac{\alpha\dot{W}_e}{\alpha_t m_t}\right)\frac{M_{tD}}{F_M\tau_b} = \left(1 + \tilde{E}_m^2\,\frac{\dot{W}_e}{\sigma_c E_m^2 A_t L}\right)\frac{M_{tD}}{F_M\tau_b} \quad (29)$$

Using Eqs. (18) and (29) we find

$$\frac{M_{f\mathrm{Th}}}{M_{\mathrm{el}D,\min}} = \left(1 + \tilde{E}_m^2\,\frac{\dot{W}_e}{\sigma_c E_m^2 A_t L}\right)\sqrt{\frac{\eta_{\mathrm{el}}\alpha v_{\mathrm{orb}}^2}{2 i_{\mathrm{av}}^2 \tilde{E}_m^4 \tau_b}} \quad (30)$$

At any given L/L^* and L_{ins}/L^*, the current i_{av} increases with the ratio $\dot{W}_e/(\sigma_c E_m^2 A_t L)$ in Eq. (9″); this results in the mass ratio in Eq. (30) presenting a minimum. At large L/L^*, that minimum occurs at $L - L_{\mathrm{ins}} \sim L^*$ and $\dot{W}_e/(\sigma_c E_m^2 A_t L)$, such that bias at the tether bottom is negligible, corresponding to values [44]

$$\alpha\dot{W}_e/\alpha_t m_t \approx 1 + \tilde{E}_m \quad (31a)$$

$$i_{\mathrm{av}}\tilde{E}_m \approx 1 \quad (31b)$$

$$\eta_t(1 + i_{\mathrm{av}}) \approx 1 \quad (31c)$$

Equations (31a) and (31b) show tether-hardware mass less than power-subsystem mass and equal to its ohmic fraction, respectively, and Eq. (31c) gives the propulsive efficiency:

$$\eta_t \equiv I_{\mathrm{av}} E_m L/\dot{W}_e = i_{\mathrm{av}} \times \sigma_c E_m^2 A L/\dot{W}_e$$

The minimum is very flat, however, allowing for some tradeoff between both subsystem masses. Note that the optimum average current in Eq. (31b) would be greater than the short-circuit current in the case of $\tilde{E}_m < 1$.

For a typical value $\tilde{E}_m \approx 1$, Eqs. (31b) and (31c) yield $i_{\mathrm{av}} \approx 1$ and $\eta_t \approx 0.5$, whereas Eq. (31a) yields a power-subsystem mass about twice the tether-hardware mass. The ratio in Eq. (30) is then three times larger than the ratio in Eq. (18). Tethers can be more mass-efficient than ion thrusters for burn times beyond 9×2.5 days, or over three weeks.

Tethers are clearly most suitable for long operations, such as for protracted drag compensation or repeatedly moving payloads to higher orbits or as space tugs that could freely deboost to meet, dock, and grapple a new payload. A study showed that a bare tether of moderate length could save, under conservative assumptions, about 80% of the chemical propellant used for reboosting the International Space Station over a 10-year lifetime, with savings estimated at $\$1 \times 109$, as presented in Fig. 9 (adapted from [45]). Tether dynamics and thrusting, however, raised concerns about impact on microgravity payloads and, in general, raised safety issues about shuttle rendezvous and flight path [46].

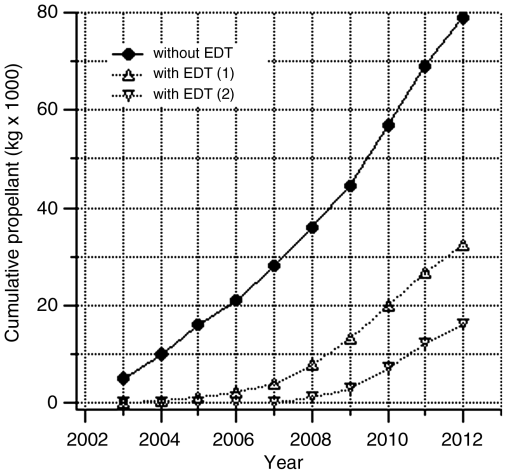

Fig. 9 Savings in propellant mass for International Space Station reboost with tether at 50 and 80% duty cycle [lines EDT(1) and EDT(2), respectively]; from [45].

VIII. Radiation Belt Remediation

In recent years there has been increasing interest in the potential for artificial modifications of the high-energy particle population that is trapped by the Earth's magnetic field at altitudes well above those at which collisions would retard and absorb them [47,48]. This potential rests on the fact that the particle densities involved are quite small (1–100/m^3), and the natural replenishment rates from the solar wind and cosmic radiation are slow enough (lifetimes from days to years) that if a mechanism can be implemented to scatter them into their loss cone, the power needed to do this over large space volumes might not be excessive. Given the very dispersed nature of the radiation, it is clear that any device for affecting it will have to be quite large in at least some dimension, and it is here that tethers may present unique solutions. Two general approaches to RBR have been identified so far, as described next.

A. Electrostatic Scattering

First proposed by Danilov et al. [49], electrostatic scattering would use a multiple-kilometer pair of conductive bare tethers biased at potentials of the order of 1 MV with respect to each other. Since the positive tether would collect as much electron current as the negative one would collect in ion form, this negative tether would float with respect to the background at almost the full bias voltage. At this megavolt potential, the electrostatic sheath around the tether, as seen in Eq. (6a), would be several hundred meters in radius, only weakly depending on the tether radius, and with proper orientation would scatter a fraction of all high-energy electrons and ions passing through it into their respective loss cones. At the same time, if the wire diameter can be kept very small, the collected current, which determines the power needed to maintain the bias, can be made small as well. Calculations along these lines have been made by a number of authors [50,51].

As an example, we quote here some results of Zeineh [51] for a 1 MV, 10 km pair of tethers placed linearly end to end along a gravity-gradient stable vertical direction near equatorial orbit. At a 2000 km altitude, 6% of all ions or electrons crossing the negative sheath are deflected into their loss cone (the fraction drops below 1% above 6500 km). Ignoring replenishment or diffusion from above and below, the time to reduce (by a factor of 10) the population of a 20 km layer centered about the tether is five months at 2000 km and increases to over six years at 6000 km. If the wire diameter were 1 mm, this arrangement would consume 100 kW. The conclusion would be that the electrostatic scattering method may be feasible for the lower reaches of the radiation belts. Considerable design issues are involved through conditions of zero Lorentz force, small torque, low electron collection, and required power; Fig. 10 shows an optimum arrangement. Hoyt and Minor [50] predicted more favorable results by using a multiwire tether structure to increase the total sheath cross section. Multiple-connection tethers involve complex dynamics [52].

B. Scattering by Waves

Instead of a large deflection happening in one pass of the charged particle near the electrostatic scattering center, one can try to induce a multiplicity of smaller deflections caused by the much weaker set of fields carried by a wave. To obtain effects that are of practical magnitude, a resonance condition is required, so that the disturbing forces can act over extended periods of time for a given particle. For electrons, this indicates the whistler band, between the lower hybrid and the electron cyclotron frequencies; resonance occurs for waves that are nearly perpendicular to the magnetic field, such that the gyro frequency for the $\boldsymbol{B}_0$ component along the wave vector matches the wave frequency f, which can then be rather low compared to the gyro frequency. These are highly dispersive waves, and their group velocity is, in fact, close to the magnetic direction even near the resonance. Typical whistler waves are in the 3 to 30 kHz very-low-frequency (VLF) band. The index of refraction n near resonance can be as high as 20–40, so that the wavelength $\lambda = c/(fn)$ is in the

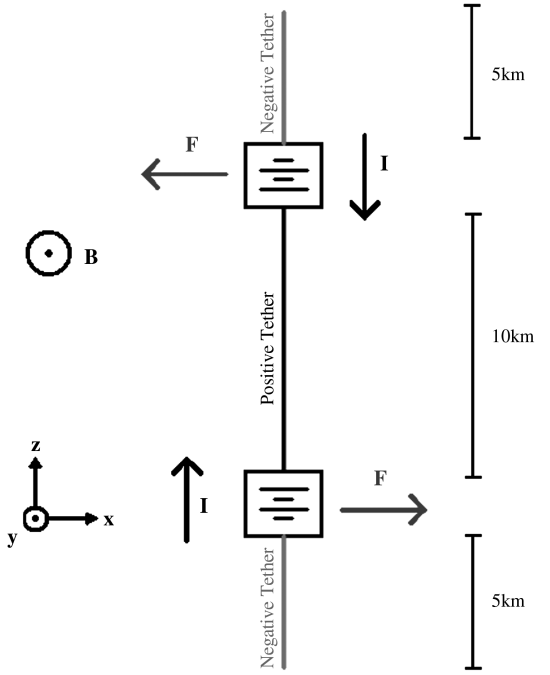

Fig. 10 Schematics of multiple tether arrangement for RBR, high-voltage scattering (from [51]).

250–5000 m range, and a half-wave electrostatic dipole antenna has a length of 125–2500 m. These are lengths that are barely practical for a rigid boom but can easily be implemented as a conductive tether. Another consequence of the high index of refraction is that the magnetic force on a particle with relativistic velocity v is $nv/c \sim n$ times larger than the electric force, so the main interaction is a deflection with no energy change. This is just what is needed to obtain over many passes through the resonance region a pitch-angle random walk that gradually diffuses particles toward the loss-cone boundary.

Calculations of electron-loss rates due to several of the known natural mechanisms involving whistler waves or Coulomb scattering, plus the effect of a few high-power VLF ground antennas have been published [53–55], with the significant result that these man-made wave injections are, in some cases, the dominant depletion channel. Recent observational confirmation was obtained by the Demeter satellite [56], which measured energetic electron populations at a 720 km altitude. Two eastern-drifting plumes of such electrons were seen starting from the location in western Australia of a 1 MW, 20 kHz U.S. Navy antenna and from its northern hemisphere conjugate point. Evidently, electrons that would normally have bounced back at higher altitudes were being scattered into their loss cone and had penetrated to the measurement altitude.

The use of these ground stations for intentional cleanup of the belts is very inefficient, since the kilohertz waves are reflected by the ionosphere, and only a small fraction (order of 1% or less near the equator) of the EM power can be coupled through plasma ducts to whistler radiation. On the other hand, in situ emission by an orbiting spacecraft carrying a very long antenna appears to be a practical proposition. The U.S. Air Force DSX spacecraft will test this idea in 2010, using a 1 kW, 80 m antenna onboard [57].

IX. Auroral Effects from Tethers

A bare tether over 10 km long left electrically floating (i.e., using electric contact device at no tether end) in low Earth orbit would be an effective electron beam source to produce artificial auroras. Because current will vanish at both ends and the ion-to-electron mass ratio is large, the tether would be biased highly negative and attract ions except at an upper segment that is a fraction $(m_e/m_i)^{1/3} \approx 0.03$ of the total length. Ions impacting with kiloelectron-volt energies would liberate secondary electrons, which would locally accelerate away from the tether, then race down geomagnetic lines and excite and ionize neutrals, resulting in auroral emissions at the ionospheric E-layer. Beyond auroral effects proper, observations down the beam from the spacecraft carrying the tether could provide real-time mapping of density profiles for dominant neutral species in the lower thermosphere, of interest for numerical simulations of the atmosphere lying below and in reentry predictions [58].

Since 1969, electron beam sources onboard spacecraft have been used in active experiments for producing artificial auroras, but such standard e-beams are marred in several ways [59]. Beam-firing affects the S/C potential serving as ground for the beam source. Large perturbations produced by the intense emission in plasma around the S/C affect the beam itself, and the luminous glow arising from electron bombardment in the return current contaminates optical instruments. Beam flux up to two orders of magnitude greater than in the strongest natural auroras compensates for the thinness of the emitting layer and makes ground observation possible; high-flux beams, however, produce hot electrons and plasma fluctuations and are distorted by nonlinear plasma interactions [60,61].

The e-beam from a tether is free from S/C charging effects, and beam emission takes place far from any instrument. The beam is also free from plasma-interaction problems, with beam density and flux being low. With secondary yield roughly proportional to bias in the range of interest, the secondary current scales as $wL^{3/2} \times L$, and the beam cross section scales as $L \times L^{1/2}$, with the width across the beam being about twice the electron gyroradius: $\propto (\text{energy})^{1/2}$. The beam flux, scaling as wL, is then well below 10^{-3} times the ambient plasma flux at emission conditions. The beam-to-ambient electron density ratio can be less than 10^{-5}.

The tether low-flux thin beam exhibits brightness for ground observation as low as 1 R (rayleigh), with light sources in the night sky masking such signals. On the other hand, brightness is much greater for observation from the spacecraf: over 10^2 R for prominent bands and lines (say, 427.8 or 391.4 nm for N_2 and 777.4 and 844.6 for O and O_2), with brightness roughly proportional to both tape width and length. This allows continuous measurements, which is impractical for the thin cross section of a standard beam, but the tether beam has one cross-sectional dimension of order of the tether length, or about 10^4 m.

Each point in the tether, which is deployed downward, emits monoenergetic secondary electrons, but both electron flux and energy increase near linearly with distance s from the top of the tether. As sketched in Fig. 11 (from [62]), observations from the spacecraft along any straight line at angle ψ from the magnetic field direction, covering some altitude range over the emission region, would mix altitude/point s effects. The narrow beam footprint in the emitting layer will then show a peak in brightness versus angle ψ about 6 deg wide, allowing tomography analysis of the signal. Results from particular calculations are shown in Fig. 12 (from [62]).

Originally, the JAXA mission mentioned in Sec. III contemplated night launch to allow a rough test of the tether e-beam aurora at the

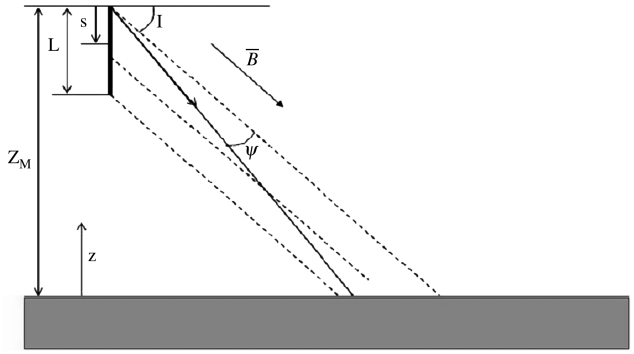

Fig. 11 Observation schematics for auroral emissions from a tether generated e-beam; *I* is here magnetic dip angle. Reproduced by permission of American Geophysical Union from [62]; copyright 2006, AGU.

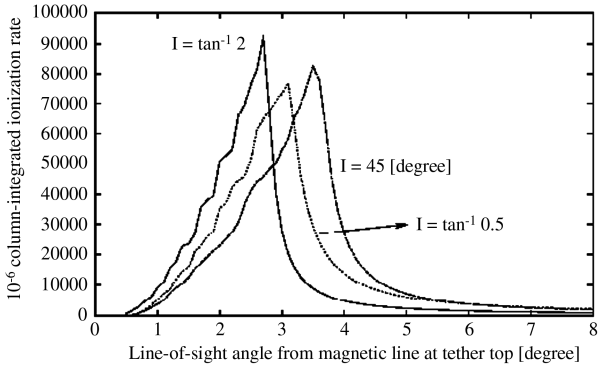

Fig. 12 Peak in auroral emission brightness versus angle away from magnetic field. Reproduced by permission of American Geophysical Union from [62]; copyright 2006, AGU.

boom-tape connection in Fig. 5, but its S-520-25 rocket will be finally launched at dawn.

X. Tether Heating

The energy equation for the temperature $T(s)$ of a tape element of length δs during the daytime can be written as

$$A_t \delta s \rho c_{\text{th}} \frac{\partial T}{\partial t} = \delta \dot{W}_{\text{th}} + \frac{p}{\pi} \delta s \alpha_{\text{abs}} S - p \delta s \varepsilon_{\text{emis}} \sigma_B T^4 \tag{32}$$

Equation (32) is a local balance, because thermal diffusivity for aluminum is of order 10^{-4} m^2/s, which is orders of magnitude smaller than, say, any reasonable value for the ratio between L^2 and a characteristic time for changes in ambient or tether conditions. In Eq. (32), which is valid for both tapes and round wires, c_{th} is specific heat, α_{abs} is absorptivity, $\varepsilon_{\text{emis}}$ is emissivity, and $S \approx 1.37$ kW/m^2 is the solar constant at LEO. For a tape, the $2/\pi$ factor in $p/\pi = w \times 2/\pi$ represents the random average orientation of a tape side with respect to solar rays.

Local tether heating in Eq. (32) is made of two contributions,

$$\frac{\delta \dot{W}_{\text{th}}}{\delta s} = \dot{w}_{\text{th1}} + \dot{w}_{\text{th2}} \equiv \frac{I^2(s)}{\sigma_c A_t} + \Delta V \frac{\delta I}{\delta s} \tag{33}$$

one due to ohmic dissipation from the current flowing through the element δs and a second contribution due to the energy brought up to the element by the impact of electrons collected at bias ΔV. It can be shown that integrating Eq. (33) over the entire tether length yields the Lorentz power $I_{\text{av}} E_m L$ in all generality [63]. The first (second) term of Eq. (33) vanishes at the anodic (cathodic) end and is maximum at the opposite end:

$$\text{Max } \dot{w}_{\text{th1}} = i_C^2 \sigma_c A_t E_m^2 \tag{34a}$$

$$\text{Max } \dot{w}_{\text{th2}} = \Delta V_A e N_0 (p/\pi) \sqrt{2e \Delta V_A / m_e} \tag{34b}$$

In the simple ohmic-dominated $L \geq 4L^*$ regime, we have both $i_C = 1$ and $\Delta V_A = E_m L^*$, as discussed in Eq. (11a), and we readily find from Eq. (7) that $\dot{w}_{\text{th1}} = \dot{w}_{\text{th2}} \times 4/3$. At night, then, we use $\dot{w}_{\text{th1}}$ from Eq. (34a) with $i_C = 1$ in Eq. (32) to determine the maximum stationary temperature occurring at the cathodic end,

$$T_{\max}^4(\text{night}) = \frac{\sigma_c E_m^2}{\sigma_B \varepsilon_{\text{emis}}} \frac{A_t}{p} \tag{35}$$

yielding $T_{\max} \approx 204$ K for a tape of thickness 0.05 mm, and $T_{\max} \approx 319$ K for a wire with the radius (0.6 mm) of the ProSEDS tether for any $L \geq 4L^*$. We used the typical LEO value, $E_m = 150$ V/km, and a representative pure-Al emissivity, $\varepsilon_{\text{emis}} = 0.2$.

Moving from eclipse to noneclipse conditions, the characteristic heating rate away from the stationary night temperature in Eq. (32) would be

$$\frac{\partial T}{\partial t} \sim \frac{p}{\pi A_t} \frac{\alpha_{\text{abs}} S}{\rho c_{\text{th}}} \tag{36}$$

Setting $\alpha_{\text{abs}} = 0.5$, we find a rate 3.64 K/s for the tape above, and 0.303 K/s for the ProSEDS wire. Next, the stationary balance in Eq. (32) yields during the daytime

$$T_{\max}^4(\text{day}) = \frac{\sigma_c E_m^2}{\sigma_B \varepsilon_{\text{emis}}} \frac{A_t}{p} + \frac{\alpha_{\text{abs}} S}{\pi \sigma_B \varepsilon_{\text{emis}}} \tag{37}$$

Note that the contribution from solar heating above is uniform along the tether and independent of its geometry. We then find $T_{\max}(\text{day}) \approx 381$ K and $T_{\max} \approx 415$ K for our tape and wire, respectively. When moving back from noneclipse to eclipse conditions, the characteristic cooling rate is again given by Eq. (36), with a minus sign.

All the above results are collected in Table 3. Note that during each orbit there are large thermal excursions on the tape, which might thus require covering with a conductive high-emissivity coating [9]. On the other hand, the wire gets significantly hotter than the tape, particularly at night, which results from the short-circuit current $\sigma_c E_m A_t$ increasing with A_t. Note the following, however:

1) At night the $L \geq 4L^*$ regime would require tethers several tens of kilometers long.

2) Wire temperature will lag the day/night equilibrium values because of the very low heating/cooling rate.

XI. Tether Bowing

Bowing due to the lateral Lorentz force is limited by tension in the tether. For a simple conservative estimate of bowing, consider the classical equation of statics for a rope under lateral load per unit length $\delta F_M / \delta s$ and supported at the two ends, with the tension assumed to be large enough to keep deflections small:

$$\frac{\mathrm{d}^2 y}{\mathrm{d}s^2} \approx \frac{\delta F_M / \delta s}{F_{\text{tens}}} = \frac{B_0 I(s)}{F_{\text{tens}}} \tag{38}$$

where y is the lateral deflection of the rope and F_{tens} is the tensile force, as sketched in Fig. 13. Here, the distributed lateral load is the Lorentz force per unit tether length, and s is measured from the anodic end, as done previously.

In the ohmic-dominated limit we would have a current $\sigma_c E_m A_t$, uniform over near the entire tether length. Integrating Eq. (38) twice with boundary conditions $y(0) = y(L) = 0$ yields the classical result for uniform load distribution, with maximum bowing (at midpoint, $s = L/2$):

$$|y|_{\max} / L = F_M / 8 F_{\text{tens}} \tag{39a}$$

Bowing in the opposite limit of weak ohmic effects is actually similar; a straightforward integration of Eq. (38) using the corresponding current law yields a quite similar maximum bowing:

Table 3 Maximum heating/cooling rates, maximum day/night temperatures at $L \geq 4L^*$ regime, and characteristic L^* values[a]

Aluminum tether type	Heating/cooling rate	$(L \geq 4L^*)\ T_{\max}$ (day)	$(L \geq 4L^*)\ T_{\max}$ (night)	$4L^*$ ($N_0 = 10^{12}$/m^3)	$4L^*$ ($N_0 = 10^{11}$/m^3)
0.05-mm-thick tape	3.64 K/s	381 K	204 K	1.65 km	7.66 km
0.6-mm-radius wire (ProSEDS tether)	0.30 K/s	415 K	319 K	8.64 km	40.20 km

[a]Values $E_m = 150$ V/km, $\alpha_{\text{abs}} = 0.5$, and $\varepsilon_{\text{emis}} = 0.2$ were used in Eqs. (35–37).

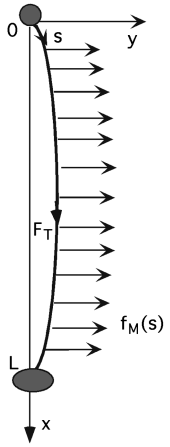

Fig. 13 Bowing of tether due to the Lorentz force; f_M is (magnetic) load per unit length, IB.

$$I(s) \propto 1-(1-s/L)^{3/2} \Rightarrow \qquad |y|_{\max}/L = F_M/7.6F_{\text{tens}} \quad (\text{at } s \approx 0.564L) \tag{39b}$$

The gravity-gradient force can provide the tension required to keep a tether taut in circular orbit around a planet in situations with moderate lateral loads. The standard formula for the gravity-gradient tensile force on a tether kept straight along the local vertical while in a quasi-circular orbit under negligible lateral force is

$$F_{\text{tens}} = 3\Omega_{\text{orb}}^2 L M_{\text{SC}}/4 \tag{40}$$

where Ω_{orb} is the orbital angular velocity, and a massless tether and equal end masses $M_{\text{SC}}/2$ are considered. Two-thirds of this tension arise from the fact that gravitational forces decrease as the inverse square of distance from the planet center. Taking into account tether mass yields a small correction that makes the tension vary with distance $(L/2)-s$ from midtether; averaging over the tether length for simple estimates just requires a correction $M_{\text{SC}} \rightarrow M_{\text{SC}} - (2m_t/3)$, which we ignore here. The tensile stress $F_{\text{tens}}/A_t \propto L^2 M_{\text{SC}}/m_t$ lies typically well below the tensile strength of aluminum.

Using Eqs. (39a) with the Lorentz force $\sigma_c E_m A_t L B_0$ and Eq. (40), we would have

$$\frac{|y|_{\max}}{L} = \frac{\sigma_c E_m^2}{6v_{\text{orb}} \times \rho\Omega_{\text{orb}}^2 L} \frac{m_t}{M_{\text{SC}}} \tag{41}$$

For $M_{\text{SC}} > 10m_t$, $L = 10$ km, and typical values for the other parameters in LEO, Eq. (41) gives a bowing ratio of about 0.05. In general, the bowing ratio at the maximum current carried by a tether would usually be small.

XII. Environment Interactions

In a plasma with no high-energy charges, as in LEO, arcing may occur at triple points, which are junctions at which conductor, dielectric, and ambient plasma are present. In the critical case, the conductor is biased highly negative relative to the ambient plasma. This may be of particular interest for tethers, with an example being the tether prepared for NASA's ProSEDS mission, planned for but finally cancelled in 2003. ProSEDS had 10 km of nonconductive material and 5 km of aluminum. A 200 m segment of this conductive tether, next to the deployer/canister, carried an insulated coating.

There were two triple points in the ProSEDS tether: one at the transition between conductive (bare) and nonconductive segments; this would be positively biased relative to the plasma, and no arcing was found in laboratory tests. There was a second triple point at the transition between conductive (bare) and conductive (insulated) segments; bias could be negative in the operational scheme. Arcing did occur at ProSEDS samples of that transition region when bias was negative enough. Arcing did also occur at pinholes (insulation breaches) arranged for testing. Arcing mitigation at the above triple point involved local covering with a semiconductor sleeve [64].

In geostationary orbit (GEO), in which high-energy electrons may be present, arcing may exhibit *snapover* and *flashover*, both phenomena related to the fact that insulators may have high secondary electrons yield [65]. Snapover again involves three elements: plasma, a positively charged conductor, and an insulator surface next to it. Attracted electrons missing the conductor may hit the insulator; secondary electrons emitted by the insulator may then be collected by the conductor. In this way, a collecting surface greater than the conductor surface itself does result. The surface of the insulator is said to be snapped over. Current may be much greater than in the absence of the insulator, and the bombarded surface may glow if the plasma density is high enough and may lead to permanent damage.

Flashover may occur after a magnetic substorm, with a conductive surface in a spacecraft in GEO then being charged negatively by energetic electrons. On the other hand, an insulator next to the conductor might be charged positively by the intense electron secondary emission due to the incident electrons. This condition is called an inverted potential gradient. As the potential difference reaches a threshold, an electrostatic discharge through breakdown in the insulator may occur. In turn, this triggers a blowoff discharge between conductor and space plasma. A flashover discharge then occurs as the now negatively charged plasma travels over the insulator, neutralizing its original positive charge [66].

An ionization-induced instability might occur at the sheath of a body biased highly positive, though only at low ionospheric altitudes at which neutral density is high enough. As attracted electrons falling through the sheath ionize neutrals, new ions move outward, resulting in an explosive growth of the sheath [67]. Originally, a large 3-D body (compared with the Debye length) was considered. The 2-D, $\lambda_{\text{De}} \approx R$ case, appropriate to bare tethers, has been recently tested in the laboratory [68], showing the instability to only occur at neutrals' densities well above values appropriate for tether operation.

Although tethers might be efficiently used to keep space clean of debris, they may also be dangerously hit by debris and micrometeorites; further, they may themselves be dangerous to manned spacecraft such as the International Space Station. The actual survival case for tethers varies from the four- to five-day life of SEDS-2 to over 10 years for the Tether Physics and Survivability Experiment, which was shorter and thicker, and at higher orbital inclination and altitude. Models for debris flux, though heavily dependent on size, show it peaking at 800–1000 km altitude and again at around 1500 km, whereas micrometeorite flux is roughly uniform in altitude [69,70]. For tape tethers, the survival probability is hard to model because it involves two characteristic cross-sectional sizes: width and thickness.

XIII. Tether Deployment

Deployment strategies are determined by orbital conditions and the desired state of the tether system at the end of the maneuver. A deployment with a librating tether will be most suitable for a system that has to end up aligned with the local vertical. Conversely, a spinning deployment is the natural choice for a system that needs to spin after deployment is complete. A librating deployment requires a relatively strong gravity gradient (e.g., in LEO) to keep the tether straight and bound to librate (or stay aligned) with the local vertical. Gravity gradient is not an issue for spinning deployments and in several applications may actually be a disturbance to the dynamics of the system.

Deployment and retrieval were studied by many authors starting in the 1970s [71–73] and 1980s [74,75] for free-flying tethered satellites, and later studies were focused on the shuttle-based tethered satellite system (TSS) [76].

Tether deployments in flight missions have thus far taken place in LEO and used the librating-deployment strategy [77,78]. In a librating deployment there are no significant centrifugal forces (due to spin) and the tether tension may need to be increased in the early stages of deployment by a thruster firing along the tether line.

Alternatively, one can reduce the time spent at short tether length by ejecting the daughter satellite at relatively high speed and very low tension in close-to-free-flying conditions [79]. Subsequently, the deployer will start braking on the tether once a significant tether length has been reached and tension due to gravity gradient takes over. An example of a librating deployment was the one followed by the SEDS-II mission in 1994. Figure 14 (adapted from [80]) shows the tether length profile vs time.

In spinning deployment, centrifugal forces generated by the spin provide tension to facilitate the extraction of the tether from the deployer. A spinning deployment can be faster than a librating deployment, because there are no limits imposed on the tether exit velocity by the maximum amplitude of a stable libration. Spinning deployments have not been experimented in space yet, but they have been studied by several authors [81,82] and their realization is expected to be quite straightforward.

In a possible scenario, the two end masses are separated initially at a relatively low speed, the system is then put into a spin by lateral thrusters placed on the end masses, and the tether exits the deployer pulled by the centrifugal forces while the tether speed is controlled by a braking mechanism. Alternatively, the end masses could be separated at high speed by exceeding the condition of librational stability and hence forcing the system to spin slowly. Lateral forces will still be needed to sustain the spin at the desired spin rate as the tether length and the moment inertia of the system increase [83]. An important advantage of the spinning deployment is that the presence of a gravity gradient is not required and, consequently, a spinning deployment can take place in deep space or, more generally, in conditions of weak gravity gradient.

Deployment of tethered systems is carried out by using passive or active deployers, in which passive stands for nonmotorized systems and active stands for motorized systems. When designed properly, a passive system is much lighter and simpler than an active deployer. Active deployers must be used for systems that need to be retrieved (e.g., the TSS missions) or for systems in which the tether length must be shortened during the mission. Otherwise, a passive deployer is well suited for deploying the tether and keeping the tether length stationary [as in the Small Expendable Deployer System [SEDS], PMG, and Young Engineers' Satellite 2 (YES2) [84] missions).

The other distinguishing factor for deployers is the mechanical design. Deployers can use a drum to reel out and in (if necessary) the tether, which is spooled on the reel. For tether retrievals, a leveling mechanism is required to distribute the tether evenly along the axis of the drum.

Passive deployers use a stationary spool whereby the tether unravels from the spool along the spool's axis. These deployers (e.g., the SEDS deployer [85]) cannot reel in the tether but they are very simple and light. Moreover, in a stationary spool the only moving mass is the exiting portion of the tether mass and, consequently, the tether can tolerate sudden accelerations without incurring high tensions. On the contrary, in a reeling deployer the whole moment of inertia of the drum is accelerated and strong tensions are unavoidable, due to strong accelerations.

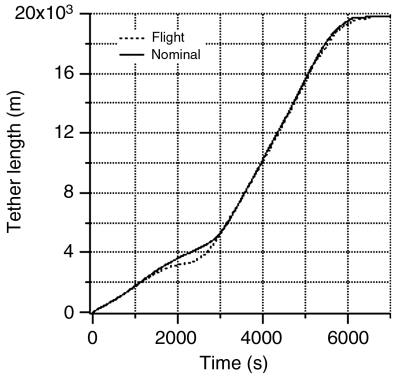

Fig. 14 Deployment length profile of SEDS-II tether mission; from [80].

In the case of a wide tape, a reeling system seems preferable to a stationary spool, because the wide tape could be twisted while exiting along the axis of the stationary spool and would be likely to produce high friction or even to cause jamming. The ATEx deployer [86] was designed to deploy a 1-in.-wide (nonconductive) tape by using a passive reel with motorized pinch rollers to pull out the tether. The addition of an in-line thruster would make this deployment scheme more tolerant of frictional forces.

The JAXA S-520-25 rocket mission will use a novel deployment strategy [87]. The tape is folded and stacked as with the long hoses used by firefighters. After spring ejection, length deployed is measured by counting folds as they approach the exit guide; deployment velocity decreases from an initial value over 3 m/s. The 300-m-long tape is fully deployed in 120 s. Deployment was tested in parabolic flight.

XIV. Issues of Present Interest

Definite results are lacking on interference effects for multiline tethers [28,88], which could increase survival probability, and on possible magnetic effects in current collection at ambient electron gyroradius well above both Debye length and probe radius. A more basic issue arises from the mesothermal character of the relative plasma flow around a tether in LEO. At the usual highly positive bias a paradox is raised. The ambient distribution of electrons would be nearly isotropic, for which a fundamental result by Laframboise and Parker [27] shows their density never exceeding the undisturbed value N_0. On the other hand, the high bias would ram back the hypersonic ions in a front region, making their density greater than N_0 over distances much larger than λ_{De}. It was suggested that satisfying quasi-neutrality as required might involve adiabatic electron trapping, which is a basic phenomenon in collisionless plasmas [89–91].

Regarding RBR, ion precipitation can be as important as electron precipitation, but it has received much less attention. The counterpart of the whistler band, the EMIC band (electromagnetic ion cyclotron), would need to be exploited. The ion cyclotron resonance can be approached only below the ion cyclotron frequency, which may be as large as 200 Hz for protons in regions of interest. Following an argument similar to that for whistlers, antennas that are 10–100 times longer (namely, multiple kilometers in length) will be needed; this can only be achieved in space using tethers.

Use of tethers at Jupiter presents a number of important novelties. Insertion in orbit [63], and touring the Jovian moons afterward [92], which are basic applications of interest, have been proved possible using the full Divine–Garrett model [93], a tens-of-kilometers-long tape with mass a sensible fraction of the full spacecraft mass being required. Radiation dose accumulated at the repeated passes through the Jovian radiation belts appears as the main limiting factor for missions that must cross the belts frequently. Typical power needs may be generated with tethers of moderate size and little effect on orbital dynamics because of the giant gravitational well of Jupiter [14]. The radiation impedance of a tether carrying a steady current, which is negligible at LEO, could be two–three orders of magnitude greater in Jupiter because of its low plasma density and strong magnetic field [94], both affecting the tether current circuit and making signal applications possible.

An array of extremely thin bare tethers was recently proposed as a new type of solar sail, using the dynamic pressure in the solar wind for interplanetary propulsion [95]. Because the sheath of each tether will be much larger than its radius, as follows from Eq. (6a), electric solar sailing may be quite efficient; the tether array, constituting a *virtual sail*, could be comparatively light. The Coulomb drag is dominant here against the Lorentz drag, because motional field, along with local magnetic field, is small, whereas very high tether voltages are required as in RBR. Sailing operations and engineering have been discussed in detail [96].

It has been suggested that current modulation in tethers would generate nonlinear low-frequency wave structures attached to the spacecraft [97]. A *magnetic pumping* process, through magnetic oscillations in the near field of the radiated wave, could result in a

parametric instability. Parallel tethers in a planar array with proper tether and mesh sizes would excite whistlers, whereas a circular array could excite an Alfvèn-wave structure.

XV. Conclusions

We have reviewed space applications of electrodynamic tethers and basic issues and constraints on their operation. We reconsidered the bare tether as an effective device solving the problem of electron collection from a rarefied magnetized plasma; thin tapes that collect as much current as round wires prove to be much lighter. We have shown that bare electrodynamic tethers in LEO can be more mass-efficient than their direct competitor, the ion thruster, for mission times that are longer than a few days for deorbiting (about 10 days for a tether also generating power) and three weeks for reboost. Also, in absence of solar power, a combined use of tether and chemical rocket is again more fuel-mass-efficient in power generation than direct use of fuel cells for times longer than one week.

We briefly recalled other tether applications, such as radiation belt remediation and generation of electron beams for atmospheric research, tether use for power and propulsion at Jupiter and electric sailing in the solar wind, and tether current modulation to generate nonlinear wave structures. Heating, arcing, and breaking, as well deployment strategies, were discussed. Tether bowing in non-spinning tethers in LEO is small if the ratio of tether mass to tip mass is small. Spinning tethers must be used in most cases at Jupiter because of the strong magnetic field and the comparatively small gravity gradient around the planet.

Acknowledgments

Work by J. R. Sanmartin was supported by the Spanish Ministerio de Ciencia y Tecnologia under grant ESP2004-01511. Work by E. Lorenzini was supported by the Centro Interdipartimentale di Studi ed Attivitá Spaziali, G. Colombo Research Center, of the University of Padova.

References

[1] Grossi, M. D., "Tether History and Historiography," *Proceedings of the 2nd International Conference on Tethers in Space*, Società Italiana di Fisica, Venice, Italy, 1987, pp. 3–8.

[2] Cosmo, M. L., and Lorenzini, E. C., *Tethers in Space Handbook*, 3rd ed., Smithsonian Astrophysical Observatory, Cambridge, MA, 1997.

[3] Laframboise, J. G., "Current Collection by a Positively Charged Spacecraft: Effects of Its Magnetic Presheath," *Journal of Geophysical Research*, Vol. 102, No. A2, 1997, pp. 2417–2432. doi:10.1029/96JA02710

[4] Vannaroni, G., Dobrowolny, M., Lebreton, J.-P., Melchioni, E., De Venuto, F., Harvey, C.C., et al., "Current-Voltage Characteristics of the TSS-1R Satellite: Comparison with Isotropic and Anisotropic Models," *Geophysical Research Letters*, Vol. 25, No. 5, 1998, pp. 749–752. doi:10.1029/97GL02577

[5] Cooke, D. L., and Katz, I., "TSS-1R Electron Currents: Magnetic Limited Collection from a Heated Presheath," *Geophysical Research Letters*, Vol. 25, No. 5, 1998, pp. 753–756. doi:10.1029/97GL03102

[6] McCoy, J.E., O'Neill, C., Stanley, J., Settecerri, T., Grossi, M., Estes, R., et al., "Plasma Motor Generator (PMG) Flight Experiment Results," *Proceedings of the Fourth International Conference on Tethers in Space*, Vol. 1; Smithsonian Institution, Washington DC, 1995, pp. 57–82.

[7] Sanmartin, J. R., Ahedo, E., and Martinez-Sanchez, M., "An Anodeless Tether Generator," *Proceedings of Workshop on Physics of Charged Bodies in Space Plasmas*, edited by M. Dobrowolny, and E. Sindoni, Società Italiana di Fisica, Varenna, Italy, 1991, pp. 201–208.

[8] Sanmartin, J. R., Martinez-Sanchez, M., and Ahedo, E., "Bare Wire Anodes for Electrodynamic Tethers," *Journal of Propulsion and Power*, Vol. 9, No. 3, 1993, pp. 353–360. doi:10.2514/3.23629

[9] Johnson, L., Estes, R. D., Lorenzini, E. C., Martinez-Sanchez, M., and Sanmartin, J. R., "Propulsive Small Expendable Deployer System Experiment," *Journal of Spacecraft and Rockets*, Vol. 37, No. 2, 2000, pp. 173–176. doi:10.2514/2.3563

[10] Carroll, J. A., "Tether Applications in Space Transportation," *Acta Astronautica*, Vol. 13, No. 4, 1986, pp. 165–174. doi:10.1016/0094-5765(86)90061-5

[11] Martinez-Sanchez, M., and Hastings, D., "A Systems Study of a 100 kW Electrodynamic Tether," *Journal of the Astronautical Sciences*, Vol. 35, No. 1, 1987, pp. 75–96.

[12] Sanmartin, J. R., and Lorenzini, E. C., "Role of Superconducting Shields in Electrodynamic Propulsion," *Journal of Propulsion and Power*, Vol. 24, No. 4, 2008, pp. 851–854. doi:10.2514/1.30433

[13] Sanmartin, J. R., and Lorenzini, E. C., "Exploration of Outer Planets Using Tethers for Power and Propulsion," *Journal of Propulsion and Power*, Vol. 21, No. 3, 2005, pp. 573–576. doi:10.2514/1.10772

[14] Bombardelli, C., Lorenzini, E. C., and Sanmartin, J. R., "Jupiter Power Generation with Electrodynamic Tethers at Constant Orbital Energy," *Journal of Propulsion and Power*, Vol. 25, No. 2, 2009, pp. 415–423. doi:10.2514/1.38764

[15] Sanmartin, J. R., Ahedo, E., Conde, L., Pelaez, J., Ruiz, M., Weinberger, M., and Hilgers, A., "Short Electrodynamic Tethers," *Proceedings of the 7th Spacecraft Charging Technology Conference*, SP-476, ESA, Noordwijk, The Netherlands, Nov. 2001, pp. 581–585.

[16] Pelaez, J., Lorenzini, E. C., Lopez-Rebollal, O., and Ruiz, M., "A New Kind of Dynamic Instability in Electrodynamic Tethers," *Journal of the Astronautical Sciences*, Vol. 48, No. 4, 2000, pp. 449–476.

[17] Wilbur, P., and Laupa, T., "Plasma Contactor Design for Electrodynamic Tether Applications," *Advances in Space Research*, Vol. 8, No. 1, 1988, pp. 221–224. doi:10.1016/0273-1177(88)90366-3

[18] Williams, J. D., and Wilbur, P. J., "Ground-Based Tests of Hollow Cathode Plasma Contactors," *Proceedings of the 3rd International Conference on Tethers in Space-Toward Flight*," AIAA, Washington, D.C., 1989, pp. 77–87.

[19] Williams, J. D., and Wilbur, P. J., "Electron Emission from a Hollow-Cathode-Based Plasma Contactor," *Journal of Spacecraft and Rockets*, Vol. 29, No. 6, 1992, pp. 820–829. doi:10.2514/3.25537

[20] Wheelock, A., Cooke, D., and Geis, M. W., "Initial Plasma Tests of the IProSEC Cathode Device," 10th Spacecraft Charging Technology Conference, Paper P37, Biarritz, France, June 2007.

[21] Wheelock, A., Cooke, D., and Geis, M., "Initial Plasma Testing of the Ion Proportional Surface Emission Cathode," AIAA Paper 08-4596, July 2008.

[22] Sanmartin, J. R., and Estes, R. D., "The Orbital-Motion-Limited Regime of Cylindrical Langmuir Probes," *Physics of Plasmas*, Vol. 6, No. 1, 1999, pp. 395–405. doi:10.1063/1.873293

[23] Estes, R. D., and Sanmartin, J. R., "Cylindrical Langmuir Probes Beyond the Orbital-Motion-Limited Regime," *Physics of Plasmas*, Vol. 7, No. 10, 2000, 4320–4325. doi:10.1063/1.1288400

[24] Sanmartin, J. R., Choinière, E., Gilchrist, B. E., Ferry, J.-B., and Martínez-Sánchez, M., "Bare Tether Sheath and Current: Comparison of Asymptotic Theory and Kinetic Simulations in a Stationary Plasma," *IEEE Transactions on Plasma Science*, Vol. 36, No. 5, 2008, pp. 2851–2858. doi:10.1109/TPS.2008.2003978

[25] Choinière, E., and Gilchrist, B., "Self-Consistent 2-D Kinetic Simulations of High-Voltage Plasma Sheaths Surrounding Ion-Attracting Conductive Cylinders in Flowing Plasmas," *IEEE Transactions on Plasma Science*, Vol. 35, No. 1, 2007, pp. 7–22. doi:10.1109/TPS.2006.889300

[26] Ferry, J. B., and Martinez-Sanchez, M., "Electron Collection by a Tether at High Potential in a Magnetized Plasma," AIAA Paper 03-4948, July 2003.

[27] Laframboise, J. G., and Parker, L. W., "Probe Design for Orbit-Limit Current Collection," *Physics of Fluids*, Vol. 16, No. 5, 1973, pp. 629–636. doi:10.1063/1.1694398

[28] Sanmartin, J. R., and Estes, R. D., "Interference of Parallel Cylindrical Langmuir Probes," *Physics of Plasmas*, Vol. 8, No. 9, 2001, pp. 4234–4239. doi:10.1063/1.1390332

[29] Onishi, T., "Numerical Study of Current Collection by an Orbiting Bare Tether," Ph.D. Dissertation, Dept. Aeronautics and Astronautics, Massachusetts Inst. of Technology, Cambridge, MA, 2002.

[30] Deux, J.-M., Batishchev, O. V., and Martinez-Sanchez, M., "Advanced Kinetic Model for Electrodynamic Space Tethers," *4th International*

Spacecraft Propulsion Conference, SP-555, ESA, Noordwijk, The Netherlands, Oct. 2004.

[31] Vannaroni, G., and De Venuto, F., "Current Collection by Bare Tether Samples in a Simulated Ionospheric Environment," Istituto di Fisica dello Spazio Interplanetario CNR Paper 2001-17, Rome, July 2001.

[32] Gilchrist, B. E., Bilen, S. G., Choinière, E., and Gallimore, A. D., "Analysis of Chamber Simulations of Long Collecting Probes in High-Speed Dense Plasmas," *IEEE Transactions on Plasma Science*, Vol. 30, No. 5, 2002, pp. 2023–2034. doi:10.1109/TPS.2002.807538

[33] Choinière, E., Bilen, S. G., Gilchrist, B. E., Furhop, K. R., and Gallimore, A. D., "Experimental Investigation of Electron Collection to Solid and Slotted Tape Probes in a High-Speed Flowing Plasma," *IEEE Transactions on Plasma Science*, Vol. 33, No. 4, 2005, pp. 1310–1323. doi:10.1109/TPS.2005.852366

[34] Bering, E. A., Koontz, S., Katz, I., Gardner, B., Evans, D., and Ferguson, D., "The Plasma Environment of the International Space Station in the Austral Summer Auroral Zone Inferred from Plasma Contactor Data," AIAA Paper 02-0935, Jan. 2002.

[35] Fujii, H. A., Takegahara, H., Oyama, K., Sasaki, S., Yamagiwa, Y., Kruijff, M., Van der Heide, E. J., Sanmartin, J. R., and Charro, M., "A Proposed Bare Tether Experiment Onboard a Sounding Rocket," AIAA Paper 04-5718, Aug. 2004.

[36] Amatucci, B., Anderson, J., Arnold, S., Bowen, J., Carroll, J., Cofey, S., et al., "CE2: A CubeSat Electron Collection Experiment," American Astronautical Society Paper AAS 09-239, Feb. 2009.

[37] Ahedo, E., and Sanmartin, J. R., "Analysis of Bare Tether Systems for Deorbiting Low-Earth-Orbit Satellites," *Journal of Spacecraft and Rockets*, Vol. 39, No. 2, 2002, pp. 198–205. doi:10.2514/2.3820

[38] Khazanov, G. V., Stone, N. H., Krivorutsky, E. N., and Liemohn, M. W., "Current-Produced Magnetic Field Effects on Current Collection," *Journal of Geophysical Research*, Vol. 105, No. A7, 2000, pp. 15,835–15,842. doi:10.1029/2000JA000039

[39] Khazanov, G. V., Stone, N. H., Krivorutsky, E. N., and Gamayunov, K. V., "Current-Induced Magnetic Field Effects on Bare Tether Current Collection: A Parametric Study," *Journal of Geophysical Research*, Vol. 106, No. A6, 2001, pp. 10,565–10,579. doi:10.1029/2000JA000345

[40] Sanmartin, J. R., and Estes, R. D., "Magnetic Self-Field Effects on Current Collection by an Ionospheric Bare Tether," *Journal of Geophysical Research*, Vol. 107, No. A11, Nov. 2002, Paper 1335. doi:10.1029/2002JA009344

[41] Martinez-Sanchez, M., and Pollard, J. E., "Spacecraft Electric Propulsion—An Overview," *Journal of Propulsion and Power*, Vol. 14, No. 5, 1998, pp. 688–699. doi:10.2514/2.5331

[42] Estes, R. D., Sanmartin, J. R., and Martinez-Sanchez, M., "Performance of Bare Tether Systems Under Varying Magnetic and Plasma Conditions," *Journal of Spacecraft and Rockets*, Vol. 37, No. 2, 2000, pp. 197–204. doi:10.2514/2.3566

[43] Sanmartin, J. R., and Lorenzini, E. C., "Spherical Collectors Versus Bare Tethers for Drag, Thrust, and Power Generation," *IEEE Transactions on Plasma Science*, Vol. 34, No. 5, 2006, pp. 2133–2139. doi:10.1109/TPS.2006.883367

[44] Sanmartin, J. R., Estes, R. D., Lorenzini, E. C., and Elaskar, S. A., "Efficiency of Electrodynamic Tether Thrusters," *Journal of Spacecraft and Rockets*, Vol. 43, No. 3, 2006, pp. 659–666. doi:10.2514/1.16174

[45] Estes, R. D., Lorenzini, E. C., Sanmartin, J. R., Pelaez, J., Martinez-Sanchez, M., and Johnson L., "Bare Tethers for Electrodynamic Spacecraft Propulsion," *Journal of Spacecraft and Rockets*, Vol. 37, No. 2, 2000, pp. 205–211. doi:10.2514/2.3567

[46] Blumer, J. H., Donahue, B. B., and Bangham, M. E., "Practicality of Using a Tether for Electrodynamic Reboost of the International Space Station," *Space Technology and Applications International Forum 2001*, edited by M. S. El-Genk, American Inst. of Physics, Melville, NY, 2001, pp. 445–451.

[47] Inan, U. S., Bell, T. F., Bortnik, J., and Albert, J. M., "Controlled Precipitation of Radiation Belt Electrons," *Journal of Geophysical Research*, Vol. 108, No. A5, May 2003, Paper 1186. doi:10.1029/2002JA009580

[48] Day, Charles, "Very Low-Frequency Radio Waves Drain Earth's Radiation Belt of Satellite-Killing Electrons," *Physics Today*, Vol. 61, No. 8, 2008, pp. 18–21. doi:10.1063/1.2970203

[49] Danilov, V. V., Elgin, B. A., Grafodatsky, O. S., and Mirnov, V. V., "High Voltage Satellite Tethers for Active Experiments in Space," *Proceedings of the 6th Spacecraft Charging Technology Conference*, U.S. Air Force Research Lab., VS-TR-20001578, Sept. 2000, pp. 165–168.

[50] Hoyt, R. P., and Minor, B. M., "Remediation of Radiation Belts Using Electrostatic Tether Structures," *Proceedings of Aerospace Conference*, Inst. of Electrical and Electronics Engineers, Piscataway, NJ, 2005, pp. 583–594. doi:10.1109/AERO.2005.1559348

[51] Zeineh, C., "Application of an Electrostatic High-Voltage Tether to Radiation Belt Remediation," M.S. Thesis, Department Aeronautics and Astronautics, Massachusetts Inst. of Technology, Cambridge, MA, 2005.

[52] Ashenberg, J., and Lorenzini, E. C., "Dynamics of a Dual-Probe Tethered System," *Journal of Guidance, Control, and Dynamics*, Vol. 20, No. 6, 1997, pp. 1265–1268. doi:10.2514/2.7600

[53] Abel, R., and Thorpe, R. M., "Electron Scattering Loss in the Earth's Inner Magnetosphere. 1. Dominant Physical Processes," *Journal of Geophysical Research*, Vol. 103, No. A2, 1998, pp 2385-2396. doi:10.1029/97JA02919

[54] Abel, R., and Thorpe, R. M., "Electron Scattering Loss in the Earth's Inner Magnetosphere. 2. Sensitivity to Model Parameters," *Journal of Geophysical Research*, Vol. 103, No. A2, 1998, pp. 2397–2407. doi:10.1029/97JA02920

[55] Albert, J. M., "Evaluation of Quasi-Linear Diffusion Coefficients for EMIC Waves in a Multi-Species Plasma," *Journal of Geophysical Research*, Vol. 108, No. A6, 2003, Paper 1249. doi:10.1029/2002JA009792

[56] Sauvaud, J-A., Maggiolo, R., Jacquey, C., Parrot, M., Berthelier, J-J., Gamble, R. J., and Rodger, C. J., "Radiation Belt Precipitation due to VLF Transmitters: Satellite Observations," *Geophysical Research Letters*, Vol. 35, May 2008, Paper L09101. doi:10.1029/2008GL033194

[57] Spanjers, G., Winter, J., Cohen, D., Adler, A., Guarneri, J., Tolliver, M., et al. "The AFRL Demonstration and Science Experiments (DSX) for DoD Space Capability in the MEO," *Proceedings of Aerospace Conference*, Inst. of Electrical and Electronics Engineers, Piscataway, NJ, July 2006, pp. 1–10. doi:10.1109/AERO.2006.1655750

[58] Martinez-Sanchez, M., and Sanmartin, J. R., "Artificial Auroral Effects from a Bare Conducting Tether," *Journal of Geophysical Research*, Vol. 102, No. A12, 1997, pp. 27,257–27,263. doi:10.1029/97JA02044

[59] Winckler, J. R., "Controlled Experiments in the Earth's Magnetosphere with Artificial Electron Beams," *Reviews of Modern Physics*, Vol. 64, No. 3, 1992, pp. 859–871. doi:10.1103/RevModPhys.64.859

[60] Strangeway, R. J., "On the Instability of a Spatially Confined Electron Beam in a Magnetized Plasma," *Journal of Plasma Physics*, Vol. 24, No. 2, 1980, pp. 193–212. doi:10.1017/S0022377800022765

[61] Mishin, E. V., and Khazanov, G. V., "Tether-Induced Airglow: Collisionless Effects," *Geophysical Research Letters*, Vol. 33, Aug. 2006, Paper L15105. doi:10.1029/2006GL026220

[62] Sanmartin, J. R., Charro, M., Pelaez, J., Tinao, I., Elaskar, S., Hilgers, A., and Martinez-Sanchez, M., "Floating Bare Tether as Upper Atmosphere Probe," *Journal of Geophysical Research*, Vol. 111, Nov. 2006, Paper A11310. doi:10.1029/2006JA011624

[63] Sanmartin, J. R., Charro, M., Lorenzini, E. C., Garret, H. B., Bombardelli, C., and Bramanti, C., "Electrodynamic Tether at Jupiter. I: Capture Operation and Constraints," *IEEE Transactions on Plasma Science*, Vol. 36, No. 5, 2008, pp. 2450–2458. doi:10.1109/TPS.2008.2002580

[64] Vaughn, J. A., Curtis, L., and Welzyn, K. J., "Plasma Interactions with a Negative Biased Electrodynamic Tether," *8th Spacecraft Charging Technology Conference*, NASA CP-2004-213091, March 2004.

[65] Hastings, D., and Garrett, H., *Spacecraft Environment Interactions*, Cambridge Univ. Press, Cambridge, England, U.K., 1996, Chap. 5.

[66] Payan, D., Sévérin, F., Catani, J-P., Roussel, J-F., Reulet, R., and Sarrail, D., "Electrostatic Discharges on Solar Arrays. Physical Model of Inverted Potential Gradient Electrostatic Discharge," *Proceedings of the 7th Spacecraft Charging Technology Conference*, SP-476, ESA, Noordwijk, The Netherlands, Nov. 2001, pp. 151–162.

[67] Cooke, D. L., and Katz, I., "Ionization-Induced Instability in an Electron-Collection Sheath," *Journal of Spacecraft and Rockets*,

Vol. 25, No. 2, 1988, pp. 132–138.
doi:10.2514/3.25961

[68] Kashihara, K., Cho, M., and Kawamoto, S., "Ground Experiments and Computer Simulations of Interaction Between Bare Tether and Plasma," *IEEE Transactions on Plasma Science*, Vol. 36, No. 5, 2008, pp. 2324–2335.
doi:10.1109/TPS.2008.2003133

[69] Matney, M., Kessler, D., and Johnson, N., "Calculation of Collision Probabilities for Space Tethers," International Astronautical Federation, Paper 00-6.5.03, Oct. 2000.

[70] Anz-Meador, P. D., "Tether-Debris Interactions in Low Earth Orbit," *Space Technology and Applications International Forum-2001*, edited by M. S. El-Genk, American Inst. of Physics, Melville, NY, 2001, 525–531.

[71] Stuiver, W., and Bainum, P. M., "A Study of Planar Deployment Control and Libration Damping of a Tethered Interferometer Satellite," *Journal of the Astronautical Sciences*, Vol. 20, No. 6, 1973, pp. 321–346.

[72] Rupp, C. C., "A Tether Tension Control Law for Tethered Satellites Deployed Along the Local Vertical," NASA TM X-64963, Sept. 1975.

[73] Modi, V. J., and Misra, A. K., "Deployment Dynamics and Control of Tethered Satellite Systems," AIAA Paper 78-1398, Aug. 1978.

[74] Bainum, P. M., and Kumar, V. K., "Optimal Control of the Shuttle-Tethered System," *Acta Astronautica*, Vol. 7, No. 12, 1980, pp. 1333–1348.
doi:10.1016/0094-5765(80)90010-7

[75] Beletskii, V. V., and Levin, E. M., "Dynamics of the Orbital Cable System," *Acta Astronautica*, Vol. 12, No. 5, 1985, pp. 285–291.
doi:10.1016/0094-5765(85)90063-3

[76] Modi, V. J., and Misra, A. K., "Deployment and Retrieval of Shuttle-Supported Tethered Satellites," *Journal of Guidance, Control, and Dynamics*, Vol. 5, No. 3, 1982, pp. 278–285.
doi:10.2514/3.56168

[77] Fuji, H. A., and Anazawa, S., "Deployment/Retrieval Control of Tethered Subsatellite Through an Optimal Path," *Journal of Guidance, Control, and Dynamics*, Vol. 17, No. 6, 1994, pp. 1292–1298.
doi:10.2514/3.21347

[78] Lorenzini, E. C., and Carroll, J. A., "In-Orbit Experimentation with the Small Expendable-Tether Deployment System," *ESA Journal*, Vol. 15, No. 1, 1991, pp. 27–33.

[79] Cosmo, M. L., Lorenzini, E. C., and Bombardelli, C., "Space Tethers as Testbeds for Spacecraft Formation-Flying," American Astronautical Society, Paper AAS 04-171, Feb. 2004.

[80] Lorenzini, E. C., Bortolami, S. B., Rupp, C. C., and Angrilli, F., "Control and Flight Performance of Tethered Satellite Small Expendable Deployment System-II," *Journal of Guidance, Control, and Dynamics*, Vol. 19, No. 5, 1996, pp. 1148–1156.
doi:10.2514/3.21757

[81] Modi, V. J., Pradham, S., and Chu, M., "Experimental Investigation of the Dynamics Of Spinning Bodies," *Proceedings of 4th International Conference on Tethers in Space*, Vol. 2, Smithsonian Inst., Washington, D.C., April 1995, pp. 1823–1835.

[82] Williams, P., "Optimal Deployment/Retrieval of a Tethered Formation Spinning in the Orbital Plane," *Journal of Spacecraft and Rockets*, Vol. 43, No. 3, 2006, pp. 638–650.
doi:10.2514/1.17093

[83] Cosmo, M. L., Lorenzini, E. C., Gramer, D. J., Hoffman, J. H., and Mazzoleni, A. P., "TESSX: A Mission for Space Exploration with Tethers," AIAA Paper 05-4288, July 2005.

[84] Kruijff, M., van der Heide, E. J., Stelzer, M., Ockels, W. J., and Gill, E., "First Mission Results of the YES2 Tethered SpaceMail Experiment," AIAA Paper 08-7385, Aug. 2008.

[85] Carroll, J., "SEDS Deployer Design and Flight Performance," *Proceedings of 4th International Conference on Tethers in Space*, Vol. 2, Smithsonian Inst., Washington, D.C., 1995, pp. 593–600.

[86] Koss, S., "Tether Deployment Mechanism for the Advanced Tether Experiment (ATEx)," *7th European Space Mechanism and Tribology Symposium*, SP-410, ESA, Noordwijk, The Netherlands, Oct. 1997.

[87] Fujii, H. A., Watanabe, T., Kojima, H., Oyama, K.-I., Kusagaya, T., Yamagiwa, Y., et al., "Sounding Rocket Experiment of Bare Electrodynamic Tether System," *Acta Astronautica*, Vol. 64, Nos. 2–3, 2009, pp. 313–324.
doi:10.1016/j.actaastro.2008.07.006

[88] Ikeda, T., Nakamura, Y., Yamagiwa, Y., Otsu, H., Kawamoto, S., Ohkawa, Y., and Nakajima, A., "Multiple Bare Tethers for Electrodynamic Tether Propulsion," Electric Rocket Propulsion Society Paper IEPC 07-280, Sept. 2007.

[89] Onishi, T., Martinez-Sanchez, M., Cooke, D. L., and Sanmartin, J. R., "PIC Computation of Electron Current Collection to a Moving Bare Tether in the Mesothermal Condition," Electric Rocket Propulsion Society Paper IEPC 01-245, Oct. 2001.

[90] Sanmartin, J. R., "Physics and Applications of Electrodynamic Space Tethers," *Simplicity, Rigor and Relevance in Fluid Mechanics*, International Centre for Numerical Methods in Engineering (CIMNE), Barcelona, 2004, pp. 316–330.

[91] Deux, J.-M., "Kinetic Modeling of Electrodynamic Space Tethers," M.S. Thesis, Dept. Aeronautics and Astronautics, Massachusetts Inst. of Technology, Cambridge, MA, 2004.

[92] Sanmartin, J. R., Charro, M., Lorenzini, E. C., Garret, H. B., Bombardelli, C., and Bramanti, C., "Electrodynamic Tether at Jupiter—II: Fast Moon Tour After Capture," *IEEE Transactions on Plasma Science*, Vol. 37, No. 4, 2009, pp. 620–626.
doi:10.1109/TPS.2009.2013955

[93] Divine, N., and Garrett, H. B., "Charged Particle Distributions in Jupiter's Magnetosphere," *Journal of Geophysical Research*, Vol. 88, No. A9, 1983, pp. 6889–6903.
doi:10.1029/JA088iA09p06889

[94] Sanchez-Torres, A., Sanmartin, J. R., Donoso, J. M., and Charro, M., "The Radiation Impedance of Electrodynamic Tethers in a Polar Jovian Orbit," *Advances in Space Research*, Vol. 45, 2010, pp. 1050–1057.
doi:10.1016/j.asr.2009.12.007

[95] Janhunen, P., "Electric Sail for Spacecraft Propulsion," *Journal of Propulsion and Power*, Vol. 20, No. 4, 2004, pp. 763–764.
doi:10.2514/1.8580

[96] Janhunen, P., and Sandroos, A., "Simulation Study of Solar Wind Push on a Charged Wire: Basis of Solar Wind Electric Sail Propulsion," *Annales Geophysicae*, Vol. 25, No. 3, 2007, pp. 755–767.

[97] Sanchez-Arriaga, G., and Sanmartin, J. R., "Magnetic Pumping of Whistler Waves by Tether Current Modulation," *Journal of Geophysical Research*, Vol. 115, 2010, Paper A02311.
doi:10.1029/2009JA014478

A. Ketsdever
Associate Editor